PCCP

ROYAL SOCIETY OF CHEMISTRY

PAPER

View Article Online
View Journal | View Issue

Cite this: *Phys. Chem. Chem. Phys.*, 2024, **26**, 6540

Can tunneling current in molecular junctions be so strongly temperature dependent to challenge a hopping mechanism? Analytical formulas answer this question and provide important insight into large area junctions

Ioan Bâldea

Analytical equations like Richardson–Dushman's or Shockley's provided a general, if simplified conceptual background, which was widely accepted in conventional electronics and made a fundamental contribution to advances in the field. In the attempt to develop a (highly desirable, but so far missing) counterpart for molecular electronics, in this work, we deduce a general analytical formula for the tunneling current through molecular junctions mediated by a single level that is valid for any bias voltage and temperature. Starting from this expression, which is exact and obviates cumbersome numerical integration, in the low and high temperature limits we also provide analytical formulas expressing the current in terms of elementary functions. They are accurate for broad model parameter ranges relevant for real molecular junctions. Within this theoretical framework we show that: (i) by varying the temperature, the tunneling current can vary by several orders of magnitude, thus debunking the myth that a strong temperature dependence of the current is evidence for a hopping mechanism, (ii) real molecular junctions can undergo a gradual (Sommerfeld–Arrhenius) transition from a weakly temperature dependent to a strongly ("exponential") temperature dependent current that can be tuned by the applied bias, and (iii) important insight into large area molecular junctions with eutectic gallium indium alloy (EGaIn) top electrodes can be gained. *E.g.*, merely based on transport data, we estimate that the current carrying molecules represent only a fraction of $f \approx 4 \times 10^{-4}$ out of the total number of molecules in a large area Au–S–$(CH_2)_{13}$–CH_3/EGaIn junction.

Received 17th October 2023,
Accepted 7th December 2023

DOI: 10.1039/d3cp05046g

rsc.li/pccp

1 Introduction

Although representing only a small fraction compared to the overwhelming majority of studies conducted at room temperature, a number of investigations on charge transport in molecular junctions at variable temperature have been carried out in the past.[1–35] Charge flow through molecular junctions can occur *via* a single-step tunneling mechanism or *via* a two-step hopping mechanism. Whether the measured current depends on temperature or not is taken by conventional wisdom as an expedient criterion to assign a specific case to hopping or tunneling, respectively. Presumably the reason why experimentalists resort(ed) to this pragmatic criterion can easily be understood. Most model theoretical approaches[36–43] were developed for zero temperature ($T = 0$) and, if at all and even if deduced for $T = 0$, compact analytical formulas enabling straightforward I–V data fitting are rather scarce.[39,43–45]

A temperature dependence of the tunneling current (I) can arise due to the thermal broadening of the electronic Fermi distribution in electrodes. Recognizing this fact, several investigations drew attention that temperature dependent transport properties are compatible with a tunneling mechanism.[1,8,23,26,32,46–53]

Still, a fundamental question remains to be addressed: is the smearing of electrodes Fermi distribution sufficient to cause a temperature dependence strong enough to compete with that generated by hopping, which is known to yield currents exhibiting an exponential Arrhenius-type variation over several orders of magnitude? From a pragmatic standpoint, equally important is another question: is it possible to meet the experimentalists' legitimate need of having compact theoretical formulas expressing the tunneling current at arbitrary temperature obviating the cumbersome numerical integration (see eqn (4) below)?

In Section 2, an analytical exact formula will be presented which enables to express the tunneling current (I) mediated by

Theoretical Chemistry, Heidelberg University, Im Neuenheimer Feld 229, D-69120 Heidelberg, Germany. E-mail: ioan.baldea@pci.uni-heidelberg.de; Fax: +49 6221 545221; Tel: +49 6221 545219

a single level at any temperature and bias in terms of digamma functions of complex argument. Based on that formula, we will show that I can indeed vary over several orders of magnitudes (Section 4), making discrimination between tunneling and hopping a challenging matter (see Conclusion). We will also deduce analytical formulas for the current expressed in terms of elementary functions valid in the low and high temperature limits (Section 3); they turn out to be very accurate in very broad model parameter ranges (Section 5), complementary covering virtually all situations of interest for real molecular junctions.

As an application, starting from experimental current–voltage data measured for a real molecular junction,[54] we will illustrate (Section 7) how a (Sommerfeld–Arrhenius[52]) transition from a current weakly varying with temperature at low T to a strongly temperature current at high T can be be controlled by tuning the applied bias voltage within a ''tunneling-throughout'' scenario.

As a by-product, we show how the presently considered single-level model of transport can provide important insight into large area molecular junctions with eutectic gallium indium alloy (EGaIn) top electrodes.

2 Model and exact formula for the current at arbitrary temperature

The Keldysh nonequilibrium formalism allows to express the tunneling current through a single molecule mediated by a single level (molecular orbital, MO) of energy ε_V by[36,55]

$$I = N\frac{2e}{h}\int_{-\infty}^{\infty} \underbrace{\Gamma_s\Gamma_t|\mathscr{G}(\varepsilon)|^2}_{\mathscr{T}(\varepsilon)}[f(\varepsilon-\mu_s)-f(\varepsilon-\mu_t)]\mathrm{d}\varepsilon \qquad (1)$$

where $f(\varepsilon) = \left[1+\exp\left(\frac{\varepsilon}{k_B T}\right)\right]^{-1}$ is the Fermi–Dirac distribution, and $\mu_{s,t} = \pm eV/2$ are the chemical potentials of the electrodes (''substrate s and ''tip/top'' t).

Key quantities in the above equation are the MO-electrode electronic couplings $\Gamma_{s,t}$, which also enter the retarded Green's function G of the embedded molecule *via* Dyson's equation

$$\mathscr{G}^{-1}(\varepsilon) = \varepsilon - \varepsilon_V + \underbrace{\frac{i}{2}(\Gamma_s+\Gamma_t+\Gamma_{env})}_{-\Sigma} \qquad (2)$$

We emphasize that although for the sake of convenience we will simply write ε_V almost everywhere, various forward-backward asymmetries can yield a bias dependent MO energy offset, *e.g.*

$$\varepsilon_V \rightarrow \varepsilon_0(V) = \varepsilon_0 + \gamma eV \qquad (3)$$

and all the formula presented below hold for a general bias dependent quantity $\varepsilon_0(V)$ not even restricted to the (linear in V) form mentioned above.

Notice that, along with electrodes' contribution $\Gamma_{s,t}$, we have also included in the Dyson eqn (2) an additional (''extrinsic'') contribution to the self-energy expressed *via* Γ_{env}. This is requested by the physical reality. Except for genuine single-molecule setups—*e.g.*, mechanically controlled break junctions (MC-BJ)—, the current carrying molecules are placed in an environment. In interaction with the surrounding—whether molecules of a solvent, neighboring molecules from a self-assembled monolayer, possibly also interaction in a cavity---the sharp delta-shape MO of an isolated molecule (gas phase) acquires a finite width quantified by Γ_{env}. The Green function $\mathscr{G}$ of eqn (2) may refer to a molecule linked to one electrode ($\Gamma_t \equiv 0$)—the case in a ultraviolet photoelectron spectroscopy (UPS) ''half-junction'' setup—or linked to two electrodes—the case of molecular junctions, whatever the (coherent one-step tunneling or incoherent two-step sequential) transport mechanism; it does not matter, a nonvanishing Γ_{env} can exist in all these cases.

Noteworthily, this reality needs not be accounted for phenomenologically. Whether referring to an UPS setup or to a molecular junction under bias the retarded Green's function (within an equilibrium formalism[56] or in a nonequilibrium Keldysh formalism,[36,55] respectively) can naturally account for this reality. In the Dyson eqn (2) underlying the present single level model, $\Gamma_{s,t}$ and Γ_{env} are accounted for on the same footing.

The assumption of a self-energy Σ independent of energy (ε)—which underlines the ubiquitous Lorentzian transmission $\mathscr{T}(\varepsilon)$—is legitimate in the case of metal electrodes possessing flat energy bands and environments without special features around the Fermi energy. In the same vein and for the sake of simplicity, we did not explicitly consider interactions of the envisaged molecule with electrodes and surrounding (see above) yielding a nonvanishing contribution to the real part of the self-energy Σ in eqn (2). All these effects amount to renormalize the value of ε_0 entering eqn (3).

$$I = \frac{2e}{h}\Gamma^2\int_{-\infty}^{\infty}\frac{f(\varepsilon-\mu_s)-f(\varepsilon-\mu_t)}{(\varepsilon-\varepsilon_V)^2+\Lambda^2}\mathrm{d}\varepsilon \qquad (4)$$

$$\Gamma^2 \equiv \Gamma_s\Gamma_t = \Gamma_g{}^2 \qquad (5)$$

$$\Lambda \equiv \frac{1}{2}(\Gamma_s+\Gamma_t+\Gamma_{env}) = \Gamma_a + \frac{\Gamma_{env}}{2} \qquad (6)$$

Notice that, after replacing Γ_a by Λ, all formulas presented in our earlier works (*e.g.*, ref. 43, 52, 53 and 57) in terms of the geometric (''effective'') and arithmetic average (Γ_g and Γ_a) remain valid although a possible contribution of the surrounding environment to the MO width (Γ_{env}) has not been explicitly mentioned. To avoid possible confusions (see ref. 58 and 57), we reiterate that the presently defined Γ's may differ by a factor of two from quantities denoted by the same symbol by other authors.

Expressed as product of a Lorentzian and a difference of Fermi function, the integrand entering eqn (4) is similar to that encountered in other phenomena (*e.g.*, superconductivity[59] or charge density waves[60]) for which contour integration is known to yield exact formulas expressed in terms of Euler's digamma function ψ of complex argument z ($\psi(z) \equiv \mathrm{d}\Gamma(z)/\mathrm{d}z$, Γ being here Euler's gamma function). Integration of eqn (4) can be

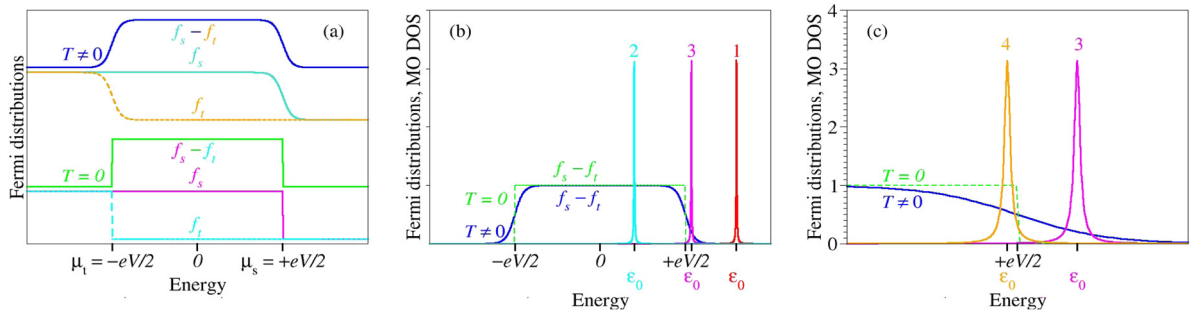

Fig. 1 (a) A nonvanishing temperature smears out the electrode Fermi distributions. (b) Negligible far away from resonance (curves 1 and 2), the effect of thermal broadening becomes important when the transmission peak comes into resonance with the electrochemical potential of one electrode (curve 3). (c) Thermal effects are more pronounced below resonance (curve 4) than above resonance (curve 3) because the overlap is larger in the former case.

carried out exactly and leads to the following form

$$I \to I_{\text{exact}} = \frac{2e\Gamma^2}{h\Lambda}\left[\operatorname{Im}\psi\left(\frac{1}{2}+\frac{\Lambda}{2\pi k_B T}+i\frac{\varepsilon_V+eV/2}{2\pi k_B T}\right) - \operatorname{Im}\psi\left(\frac{1}{2}+\frac{\Lambda}{2\pi k_B T}+i\frac{\varepsilon_V-eV/2}{2\pi k_B T}\right)\right] \tag{7}$$

Noteworthily, eqn (7) is exact at arbitrary temperature T and bias V within the single level model with Lorentzian transmission. Limitations of this model have been discussed recently[57,61] and will not be repeated here. The above formula generalizes various particular results deduced for $\Gamma_{\text{env}} \equiv 0$,[8,25,40,41,43,55,62–64] to which we will also refer below.

Putting in more physical terms, thermal fluctuations give rise to smeared Fermi distributions $f_{s,t}(\varepsilon) = f(\varepsilon - \mu_{s,t})$ in electrodes that appreciably differ from the zero temperature step (Heaviside) shape within ranges of width on the order of k_BT around the electrochemical potentials $\mu_{s,t} = \pm eV/2$ (Fig. 1a). The temperature has a negligible impact on situations wherein the energy ε_0 of dominant transport channel lies far away from resonance (curves 1 and 2 in Fig. 1b). However, the tunneling current can acquire a significant dependence on temperature in cases where a narrow enough transmission curve (*i.e.*, sufficiently small Λ) appreciably overlaps with one of the two energy ranges affected by thermal smearing (curves 3 and 4 in Fig. 1b and c). More precisely, the temperature effect is stronger in situations slightly below resonance ($\varepsilon_V \lesssim \mu_s$, curve 4 in Fig. 1c) than slightly above resonance ($\varepsilon_V \gtrsim \mu_s$, curve 3 in Fig. 1b and c). As illustrated in Fig. 1c, in the former case the current $I(\to I_{\text{exact}})$ at temperature T can be substantially larger than the current at $T = 0$ denoted by I_{0K} below (*cf.* eqn (8a)), while in the latter case I is at least half the value of I_{0K}.

3 Analytical expressions in the low and high temperature limits

3.1 Current of low temperatures

The zero temperature limit ($I \approx I_{0K}$) of eqn (7)

$$I \xrightarrow{T\to 0} I_{0K} = \frac{G_0}{e}\frac{\Gamma^2}{\Lambda}\left(\arctan\frac{\varepsilon_V+eV/2}{\Lambda}-\arctan\frac{\varepsilon_V-eV/2}{\Lambda}\right) \tag{8a}$$

is recovered using the asymptotic expansion (eqn (6.3.18) in ref. 65)

$$\psi(z)\underset{|\arg z|<\pi}{\overset{z\to\infty}{=}}\ln z+\mathcal{O}(1/z)$$

along with the identity

$$\operatorname{Im}\ln(x+iy)=\arctan\frac{y}{x}$$

An important case of the low temperature limit is the off-resonant transport, for which eqn (8a) acquires a particularly appealing form[43,57]

$$I_{0K}\underset{|\varepsilon_V\pm eV/2|\gg\Lambda}{\overset{\Lambda\ll|\varepsilon_0|}{=}}I_{0K,\text{off}}=\frac{2e^2}{h}\frac{\Gamma^2}{\varepsilon_V^2-(eV/2)^2}V \tag{8b}$$

Low temperature (thermal) corrections to current can be deduced by expanding the digamma function in powers T[65,66] or *via* Sommerfeld expansions[67,68]

$$I = I_{1,1}+\mathcal{O}(k_BT)^4; I = I_{1,2}+\mathcal{O}(k_BT)^6$$
$$I = I_{1,3}+\mathcal{O}(k_BT)^8 \tag{9a}$$

$$I \approx I_{1,1} = I_{0K}+\frac{2e}{h}\Gamma^2[c_1(\varepsilon_V+eV/2,\Lambda,T) - c_1(e_V-eV/2,L,T)](pk_BT)^2 \tag{9b}$$

$$I \approx I_{1,2} = I_{1,1}+\frac{2e}{h}\Gamma^2[c_2(\varepsilon_V+eV/2,\Lambda,T) - c_2(e_V-eV/2,L,T)](pk_BT)^4 \tag{9c}$$

$$I \approx I_{1,3} = I_{1,2}+\frac{2e}{h}\Gamma^2[c_3(\varepsilon_V+eV/2,\Lambda,T) - c_3(e_V-eV/2,L,T)](pk_BT)^6 \tag{9d}$$

where

$$c_1(\varepsilon,\Gamma,T)=-\frac{1}{3}\frac{\varepsilon}{(\varepsilon^2+\Gamma^2)^2} \tag{9e}$$

$$c_2(\varepsilon,\Gamma,T)=-\frac{7}{15}\frac{\varepsilon(\varepsilon^2-\Gamma^2)}{(\varepsilon^2+\Gamma^2)^4} \tag{9f}$$

$$c_3(\varepsilon,\Gamma,T) = -\frac{31}{63}\frac{\varepsilon\left(3\varepsilon^4 - 10\varepsilon^2\Gamma^2 + 3\Gamma^4\right)}{\left(\varepsilon^2+\Gamma^2\right)^6} \tag{9g}$$

3.2 Current at high temperatures

The identity (*cf.* eqn (6.3.12) of ref. 65)

$$\mathrm{Im}\,\psi\left(\frac{1}{2}+iy\right) = \frac{\pi}{2}\tanh\pi y$$

yields the formula for current valid in the high temperature limit $\left(\Lambda \ll \pi k_B T,\ I = I_T + \mathcal{O}\left(\frac{\Lambda}{k_B T}\right)\right)$

$$I \xrightarrow{\Lambda \ll \pi k_B T} I_T$$

$$I_T \equiv \frac{2e}{h}\frac{\Gamma^2}{\Lambda}\frac{\pi}{2}\left[\tanh\frac{\varepsilon_V + eV/2}{2k_B T} - \tanh\frac{\varepsilon_V - eV/2}{2k_B T}\right] \tag{10a}$$

$$I_T \xrightarrow{e|V|\ll 2|\varepsilon_0|} \frac{2e}{h}\frac{\Gamma^2}{\Lambda}\pi\frac{\sinh\frac{eV}{2k_B T}}{\cosh\frac{\varepsilon_V}{k_B T}} \xleftarrow{k_B T \ll e|V|\ll 2|\varepsilon_0|} I_{p.A}$$

$$I_{p.A} = \frac{2e}{h}\frac{\Gamma^2}{\Lambda}\pi\exp\left[-\frac{|\varepsilon_V| - |eV|/2}{k_B T}\right]\mathrm{sign}\,V \tag{10b}$$

Above, the subscript p.A stands for "pseudo-Arrhenius" to emphasize that, in the limit specified, the tunneling current exhibits an Arrhenius-type dependence on temperature, which is routinely (or, better, "abusively", see Introduction) considered characteristic for the hopping mechanism.

Series expansion in powers of $x \equiv \Lambda/(2\pi k_B T)$ in terms of polygamma functions $\psi(n;z) \equiv \mathrm{d}^n\psi(z)/\mathrm{d}z^n$

$$\mathrm{Im}\,\psi\left(\frac{1}{2}+x+iy\right) = \frac{\pi}{2}\tanh\pi y + x\,\mathrm{Im}\,\psi\left(1;\frac{1}{2}+iy\right) + \frac{x^2}{2}\mathrm{Im}\,\psi\left(2;\frac{1}{2}+iy\right) + \mathcal{O}\left(x^3\right) \tag{10c}$$

allows to deduce corrections to eqn (10a). Unlike the imaginary part of the tetragamma function ($\psi''(z) \equiv \psi(2;z)$), which can be expressed analytically in terms of elementary functions for $z = 1/2 + iy$

$$\mathrm{Im}\,\psi\left(2;\frac{1}{2}+iy\right) = d_2(y) \equiv -\pi^3\frac{\sinh\pi y}{\cosh^3\pi y} \tag{10d}$$

the imaginary part of the trigamma function ($\psi'(z) \equiv \psi(1;z)$) entering eqn (10c) cannot. However, we found that it can be accurately interpolated numerically (see Fig. 2a)

$$\mathrm{Im}\ \psi\left(1;\frac{1}{2}+iy\right) \simeq d_1(y) \equiv -y\left[\frac{1}{0.958287+y^2} + \frac{0.944894}{(0.244104+y^2)^2}\right] \tag{10e}$$

We thus arrive at the following expressions applicable for MO broadening smaller that the thermal smearing of electrode Fermi functions (quantified by Λ smaller than $k_B T$) characterizing transport data that exhibit a pronounced temperature dependence

$$I = I_{h,1} + \mathcal{O}\left(\frac{\Lambda}{k_B T}\right)^2;\ I = I_{h,2} + \mathcal{O}\left(\frac{\Lambda}{k_B T}\right)^3 \tag{10f}$$

$$I \approx I_{h,1} = I_T + \frac{2e}{h}\frac{\Gamma^2}{\Lambda}\frac{\Lambda}{2\pi k_B T}\left[d_1\left(\frac{\varepsilon_V + eV/2}{2\pi k_B T}\right) - d_1\left(\frac{\varepsilon_V - eV/2}{2\pi k_B T}\right)\right] \tag{10g}$$

$$I \approx I_{h,2} = I_{h,1} + \frac{2e}{h}\frac{\Gamma^2}{\Lambda}\left(\frac{\Lambda}{2\pi k_B T}\right)^2\left[d_2\left(\frac{\varepsilon_V + eV/2}{2\pi k_B T}\right) - d_2\left(\frac{\varepsilon_V - eV/2}{2\pi k_B T}\right)\right] \tag{10h}$$

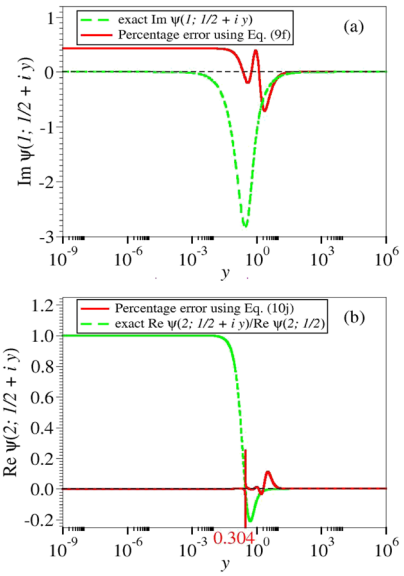

Fig. 2 The deviations of the numerical interpolation functions (a) $d_2(y)$ of eqn (10e) and (b) $\varphi(x)$ of eqn (11k) from $\mathrm{Im}\,\psi'(1/2 + iy)$ and $\mathrm{Re}\,\psi(2; 1/2 + iy)$, respectively are smaller than half of percent.

Notice that, similar to $c_{1,2,3}$ (*cf.* eqn (9e)), the quantities $d_{1,2}$ are expressed in terms of elementary functions (*cf.* eqn (10e) and (10d)). This is important for potential applications to processing transport data exhibiting substantial dependence temperature; special functions (digamma ψ in this specific case) of complex argument (*cf.* eqn (7)) are not implemented in software packages (like ORIGIN or MATLAB) routinely utilized by experimentalists for data fitting.

3.3 Analytical expressions for the zero bias conductance

In the zero bias limit ($V \to 0$), eqn (7) recovers the recently deduced formula for the exact ohmic conductance G.[52] It is expressed in terms of the trigamma function ($\psi'(z) = \mathrm{d}\psi(z)/\mathrm{d}z$)

$$G \to G_{exact} \equiv \left.\frac{\partial I_{exact}}{\partial V}\right|_{V=0} = G_0\frac{\Gamma^2}{2\pi\Lambda k_B T}\mathrm{Re}\ \psi'\left(\frac{1}{2}+\frac{\Lambda + i\varepsilon_0}{2\pi k_B T}\right) \tag{11a}$$

Thermal corrections to the zero temperature conductance G_{0K}

$$G \xrightarrow{T=0} G_{0K} \equiv G_0 \frac{\Gamma^2}{\varepsilon_0^2 + \Lambda^2} \tag{11b}$$

obtained from the asymptotic expansion of the digamma function read

$$G = G_{0K} + \mathcal{O}(k_B T)^2 \tag{11c}$$

$$\begin{aligned} G &= G_{1,1} + \mathcal{O}(k_B T)^4; \\ G &\approx G_{1,1} = G_{0K} + G_0 \Gamma^2 \frac{1}{3} \frac{3\varepsilon_0^2 - \Lambda^2}{(\varepsilon_0^2 + \Lambda^2)^3} (\pi k_B T)^2 \end{aligned} \tag{11d}$$

$$\begin{aligned} G &= G_{1,2} + \mathcal{O}(k_B T)^6; \\ G &\approx G_{1,2} = G_{1,1} + G_0 \Gamma^2 \frac{7}{15} \frac{5\varepsilon_0^4 - 10\varepsilon_0^2 \Lambda^2 + \Lambda^4}{(\varepsilon_0^2 + \Lambda^2)^5} (\pi k_B T)^4 \end{aligned} \tag{11e}$$

$$G = G_{1,3} + \mathcal{O}(k_B T)^8; \tag{11f}$$

$$G \approx G_{1,3} = G_{1,2} + G_0 \Gamma^2 \frac{31}{21} \frac{7\varepsilon_0^6 - 35\varepsilon_0^4 \Lambda^2 + 21\varepsilon_0^2 \Lambda^4 - \Lambda^6}{(\varepsilon_0^2 + \Lambda^2)^7} (\pi k_B T)^6 \tag{11g}$$

Analytical expressions in the high temperature limit (Λ smaller than $\pi k_B T$) deduced previously[52,53] are included for the reader's convenience ($y \equiv \varepsilon_0/(2\pi k_B T)$)

$$\begin{aligned} G &\xrightarrow{\Lambda \ll \pi k_B T} G_T \equiv G_0 \frac{\pi \Gamma^2}{4 \Lambda k_B T} \mathrm{sech}^2(\pi y) \\ G_T &\xrightarrow{\pi k_B T \ll |\varepsilon_0|} G_0 \frac{\pi \Gamma^2}{\Lambda k_B T} \exp\left(-\frac{|\varepsilon_0|}{k_B T}\right) \end{aligned} \tag{11h}$$

$$\begin{aligned} G &= G_{h,1} + \mathcal{O}\left(\frac{\Lambda}{\pi k_B T}\right); \\ G &\approx G_{h,1} \equiv G_T + G_0 \Gamma^2 \frac{\varphi(y)}{(2\pi k_B T)^2} \end{aligned} \tag{11i}$$

$$\begin{aligned} G &= G_{h,2} + \mathcal{O}\left(\frac{\Lambda}{\pi k_B T}\right)^2; \\ G &\approx G_{h,2} \equiv G_{h,1} + G_0 \Gamma^2 \frac{\pi}{16} \frac{\Lambda}{(k_B T)^3} \times [2 - \cosh(2\pi y)] \mathrm{sech}^4(\pi y) \end{aligned} \tag{11j}$$

$$\begin{aligned} \mathrm{Re}\,\psi\left(2; \frac{1}{2} + iy\right) \simeq \varphi(y) \equiv & \frac{y^2 - 34.7298}{(y^2 + 2.64796)^2} \\ & + 37.262 \frac{y^2 + 1.12874}{(y^2 + 2.17786)^3} \\ & + 3.01373 \frac{y^2 - 0.082815}{(y^2 + 0.25014)^3} \end{aligned} \tag{11k}$$

The high accuracy of the numerical interpolation expressed by eqn (11k) is depicted in Fig. 2b.

4 Can the temperature impact on the transport by tunneling be as strong as on the transport by hopping?

To reiterate what we have mentioned in Section 2, all the above analytical formulas deduced for the tunneling current hold for MO energy offsets $\varepsilon_0(V)$ exhibiting an arbitrary dependence on the applied bias V, including in particular the case of nonvanishing Stark strengths $\gamma \neq 0$. In this section, for simplicity, we confine ourselves to present numerical results for the bias independent case ($\varepsilon_0(V) = \varepsilon_0$, $\gamma = 0$). Because the charge conjugation invariance of this model yields equal currents computed for $+\varepsilon_0$ and $-\varepsilon_0$ and symmetric I–V curves ($I(-V) = -I(V)$), we can restrict ourselves to positive ε_0 and V without loss of generality.

As said, traditionally a strongly temperature dependent transport was considered as a fingerprint for a hopping mechanism, but we showed above that the thermal broadening of electron Fermi distributions in electrodes makes the tunneling current dependent on temperature (see also Fig. 3). Can the tunneling current expressed by the above formulas vary over orders of magnitude if the temperature varies within experimentally relevant ranges, challenging thereby the hopping mechanism or the occurrence of a tunneling-hopping transition?

The numerical results collected in Fig. 4 offer the (positive) answer to this question. The first and second columns of Fig. 4 (panels a to d and e to h, respectively) depict the thermal excess quantified by the ratio of the exact conductance G_{exact} (eqn (11a)) and the exact current I_{exact} (eqn (7)) computed at $T = 373.15$ K ($k_B T = 32.2$ meV) and several biases ($V = 0.1$; 0.5; 1.0 V) and their counterparts G_{0K} and I_{0K} at the same biases but at $T = 0$ (eqn (11b) and (8a), respectively) for the model parameter ranges

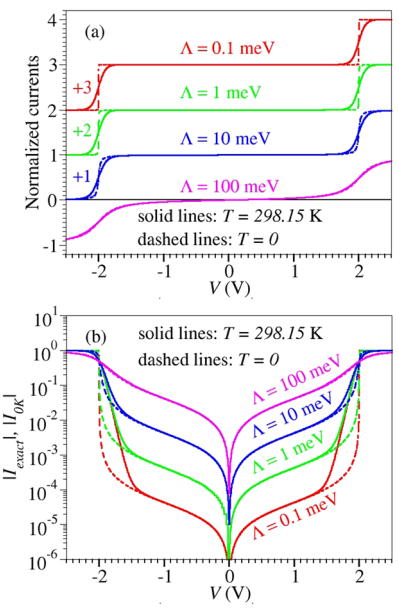

Fig. 3 Currents at T = 298.15 K (solid lines) and T = 0 (dashed lines) normalized at the plateau value $\Lambda/(\pi\Gamma^2)$ for various values of Λ in (a) linear and (b) logarithmic y scale. For clarity, in panel a they are shifted vertically as indicated in the legend.

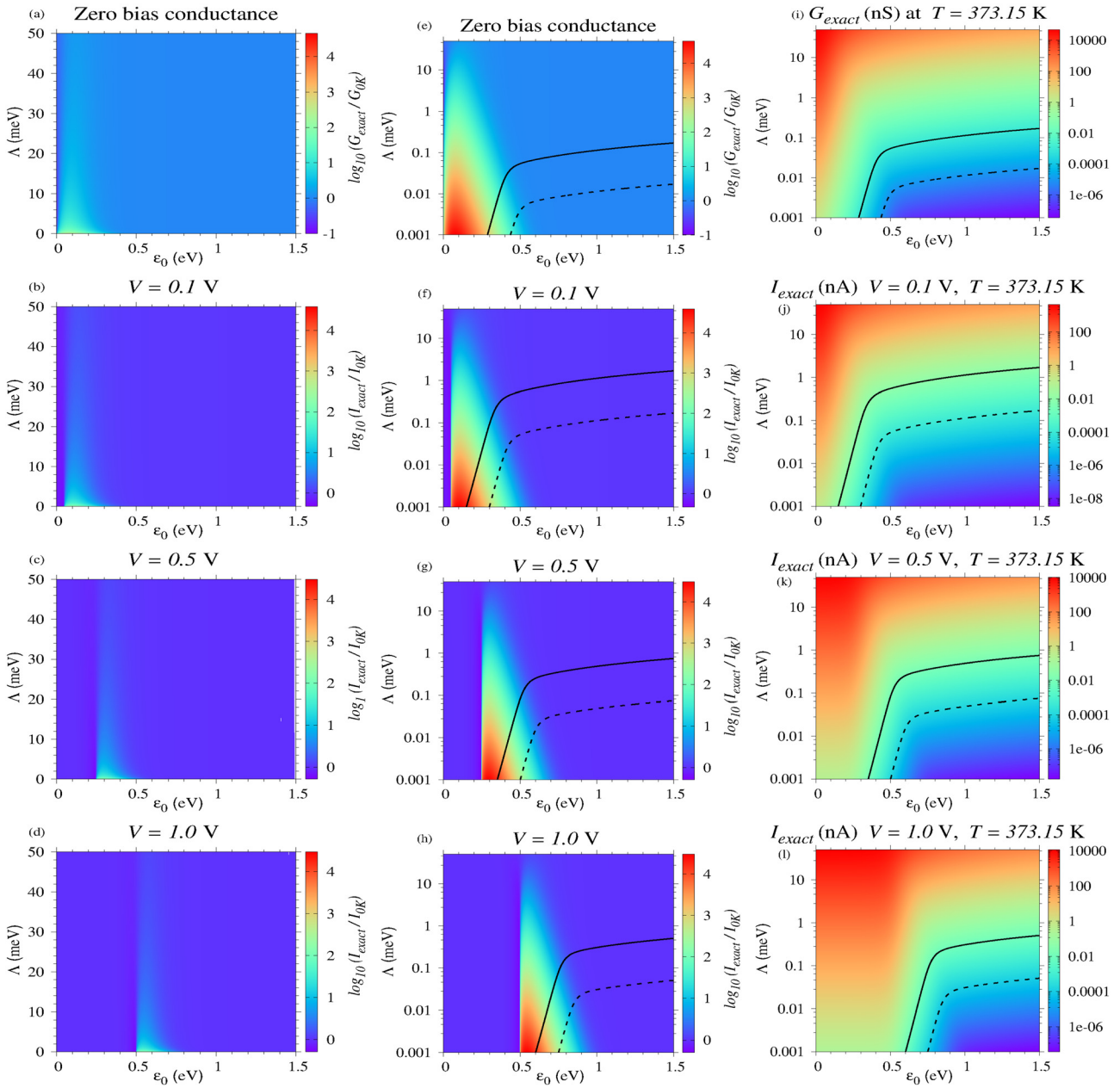

Fig. 4 (a)–(h) Ratio of the relevant transport properties (conductance G_{exact} and current I_{exact}) computed at T = 373.15 K and values of bias V indicated relative to their counterparts at T = 0 K (G_{0K} and I_{0K}, respectively). The model parameter Λ is depicted both in linear and (to better visualize the order of magnitude) logarithmic scale (panels a to d and e to h, respectively). By and large, the main effect of the bias V is a horizontal energy shift $eV/2$ of the parameter ranges corresponding to substantial thermal enhancement, which becomes more pronounced as the resonance ($\varepsilon_0 = eV/2$) is approached from below ($\varepsilon_0 \gtrsim eV/2$). Diagrams for the zero bias conductance in nS (i) and (j)–(l) current in nA at T = 373.15 K. The parameter regions wherein $G_{exact} > 1$ pS (panel i) and $I_{exact} > 10$ pA (panels j–l), which can be considered reasonable lower bound values for experimental accessibility, lie below the solid and dashed lines. See the main text for details.

1 meV $\leq \varepsilon_0 \leq$ 1.5 eV and 0.001 meV $\leq \Lambda \leq$ 50 meV. (We chose T = 373.15 K for illustration, as a reasonable value for the highest temperature of any practical interest.) Inspection of these panels indicates a current thermal enhancement up to three to four orders of magnitudes for a sufficiently small Λ and MO level outside the Fermi window but no very far away from resonance (say, $e|V|/2 < |\varepsilon_0| \lesssim e|V|/2 + 10k_BT$).

To avoid misunderstandings related to the appearance of Fig. 4, we emphasize that, unlike the current thermal excess I_{exact}/I_{0K}, which is highly asymmetric around resonance—very large below resonance ($I_{exact}/I_{0K} \gg 1$ for $e|V|/2 \lesssim |\varepsilon_0|$) but not too small above resonance ($1 > I_{exact}/I_{0K} > 1/2$ for $e|V|/2 \gtrsim |\varepsilon_0|$)—the absolute difference $|I_{exact} - I_{0K}|$ is practically symmetric around resonance ($e|V|/2 = |\varepsilon_0|$); compare Fig. 4 with Fig. 5. Along with the strong thermal enhancement, convincing oneself that the conductance/current are reasonable large to be measurable in the pertaining model parameter ranges is an equally important aspect that deserves consideration.

Therefore, Fig. 4 also indicates the parameter ranges wherein the values G and I are larger than 1 pS and 0.01 pS, and 10 pA and 0.1 pA, respectively. These values correspond to the regions above the continuous and dashed lines depicted in panels e to l. (We do not show these lines in panels a to d because the linear y-scale would make visibility problematic.) Above, the larger values 1 pS and 10 pA were chosen as realistic lowest values still measurable for single molecule junctions. The values one hundred times lower (0.01 pS and 0.1 pA) can be taken as the counterpart for CP-AFM junctions, which consist of $\sim$100 molecules per junction.[69]

To sum up, we conclude that the impact of temperature on the transport *via* a single step tunneling mechanism can definitely be as strong as that the impact on the two-step hopping mechanism, which was traditionally associated to a pronounced temperature dependence.

5 How accurate are the analytical approximations expressed in terms of elementary functions?

To illustrate the accuracy of the approximate formulas for conductance and current deduced in Section 3.3, we present comparison with the exact eqn (11a) and (7) at T = 373.15 K at several biases: V = 0; 0.1; 0.5; 1.0 V (Fig. 6–9, respectively).

Methodologically, performing (Sommerfeld) expansions in powers of T (more precisely, in even powers of T because odd powers do not contribute) is the most straightforward way to account for thermal effects on the tunneling current.[67,68] Doing so, eqn (9b)–(9d) and (11d)–(11f) can be recovered after some tedious calculations. Inspection reveals that, including the first order correction ($\propto T^2$), G_{l1}, and $I_{l,1}$ represent a better description with respect to the zero temperature quantities G_{0K} and I_{0K}; compare Fig. 6b, 7b, 8b and 9b with Fig. 6a, 7a, 8a and 9a, respectively. Still, although the second order correction ($\propto T^4$) depicted in Fig. 6c, 7c, 8c and 9c represents a further improvement, expansion in powers of k_BT/Λ inherently fails for sufficiently small Λ, when the transport strongly depends on temperature.

Unfortunately, although appealing simple, the expressions for G_T and I_T deduced in the high temperature limit (eqn (11h) and (10a)) appear to have a very restricted validity; see Fig. 6d, 7d, 8d and 9d. Below resonance, I_T is only reasonably in a very narrow parameter range. And yet, the formulas deduced by adding first and second high temperature corrections ($G_{h,1}$, $G_{h,2}$, eqn (11i) and (11j)) and $I_{h,1}$, $I_{h,2}$, (eqn (10g) and (10h)) turn out to be very accurate even in the parameter ranges where the thermal impact is very pronounced; see Fig. 6e, f, 7e, f, 8e, f, and 9d, f.

Although the main aim of the present paper is to present general analytical formulas for the current through molecular junctions mediated by a single (dominant) channel rather than discussing applications to real junctions, in the next two sections we will analyze I–V curves measured for junctions fabricated using two extreme platforms: a large area junction with top electrode of eutectic gallium indium alloy (EGaIn)[70] (Section 6) and a single-molecule junction[54] (Section 7).

6 Analyzing transport data of a specific large area EGaIn-based molecular junction

In the above presentation, emphasis was on the temperature dependence of the tunneling current. However, we also want to draw attention on an effect that did not explicitly entered the foregoing discussion: the possibility that the MO of the active molecule acquires a significant width from the surrounding medium ($\Gamma_{env} \neq 0$). Furthermore, by focusing on a specific large area EGaIn junction below, we also aim at illustrating that/how the single level model can help to determine the fraction f of the current carrying molecules N_{eff}, which represent only tiny amount of the total (nominal) number of molecules N_n in junction ($f \equiv N_{eff}/N_n \ll 1$).[21,71–74] To better underline the importance of the aforementioned, we have intentionally chosen experimental results reported for a real junction wherein the impact of temperature is negligible (*cf.* Fig. 10c): a large area EGaIn-based junction fabricated with 1-tetradecanethiol SAMs (C14T) chemisorbed on gold electrode Au–S–$(CH_2)_{13}$–CH_3/EGaIn.[70] Typically, experiments on large area molecular junctions report values for the current density $J = J(V)$ (in A cm^{-2}) rather than $I = I(V)$ (in A). For this reason, we recast eqn (7), (8a) and (8b) needed below in terms of current densities

$$J_{exact} \equiv \frac{N_{eff}}{\mathscr{A}_n} I_{exact} = \bar{\Gamma}^2 \frac{G_0}{e\Lambda}\left[\mathrm{Im}\,\psi\left(\frac{1}{2}+\frac{\Lambda}{2\pi k_B T}+i\frac{\varepsilon_V+eV/2}{2\pi k_B T}\right) - \mathrm{Im}\,\psi\left(\frac{1}{2}+\frac{\Lambda}{2\pi k_B T}+i\frac{\varepsilon_V-eV/2}{2\pi k_B T}\right)\right] \tag{12a}$$

$$J_{0K} = \bar{\Gamma}^2 \frac{G_0}{e\Lambda}\left(\arctan\frac{\varepsilon_V+eV/2}{\Lambda} - \arctan\frac{\varepsilon_V-eV/2}{\Lambda}\right) \tag{12b}$$

$$J_{0K,off} = G_0 \frac{\bar{\Gamma}^2}{\varepsilon_V^2-(eV/2)^2} V \tag{12c}$$

Here

$$\bar{\Gamma}^2 \equiv \frac{N_{eff}}{\mathscr{A}_n}\Gamma^2 = \underbrace{\frac{N_{eff}}{N_n}}_{f}\underbrace{\frac{N_n}{\mathscr{A}_n}}_{\Sigma}\Gamma^2 = f\Sigma\Gamma^2 \tag{13}$$

and Σ is the SAM coverage. Recall that ε_V entering eqn (6) is a shorthand for $\varepsilon_0(V)$, *cf.* eqn (3).

Reliable values of the parameters $\varepsilon_0\bar{\Gamma}$, and γ can be obtained by fitting the experimental I–V data with any of eqn (6), the pertaining results are presented in Table 1 and Fig. 10. Noteworthily, as reiterated again and again,[47,57,58] to correctly employ our model proposed in ref. 43, eqn (12c) should be applied to bias ranges $|V| \lesssim 1.2V_t$ (*cf.* Fig. 10d). Here, the transition voltage V_t is defined as the bias where $V^2/|I|$ is maximum (Fig. 10a). All three fitting curves successfully reproduce the measurements (*cf.* Fig. 10b). The good agreement between these methods demonstrates that in the large area Au-C14T/EaGaIn considered thermal effects are negligible

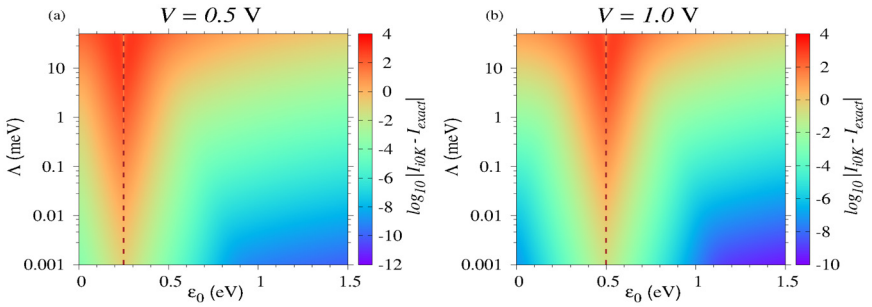

Fig. 5 Unlike the relative deviations depicted in Fig. 4, the absolute deviations of I_{0K} from I_{exact} are nearly symmetric around resonance $|\varepsilon_0| = e|V|/2$. This is illustrated here for two bias values: (a) V = 0.5 V and (b) V = 1.0 V.

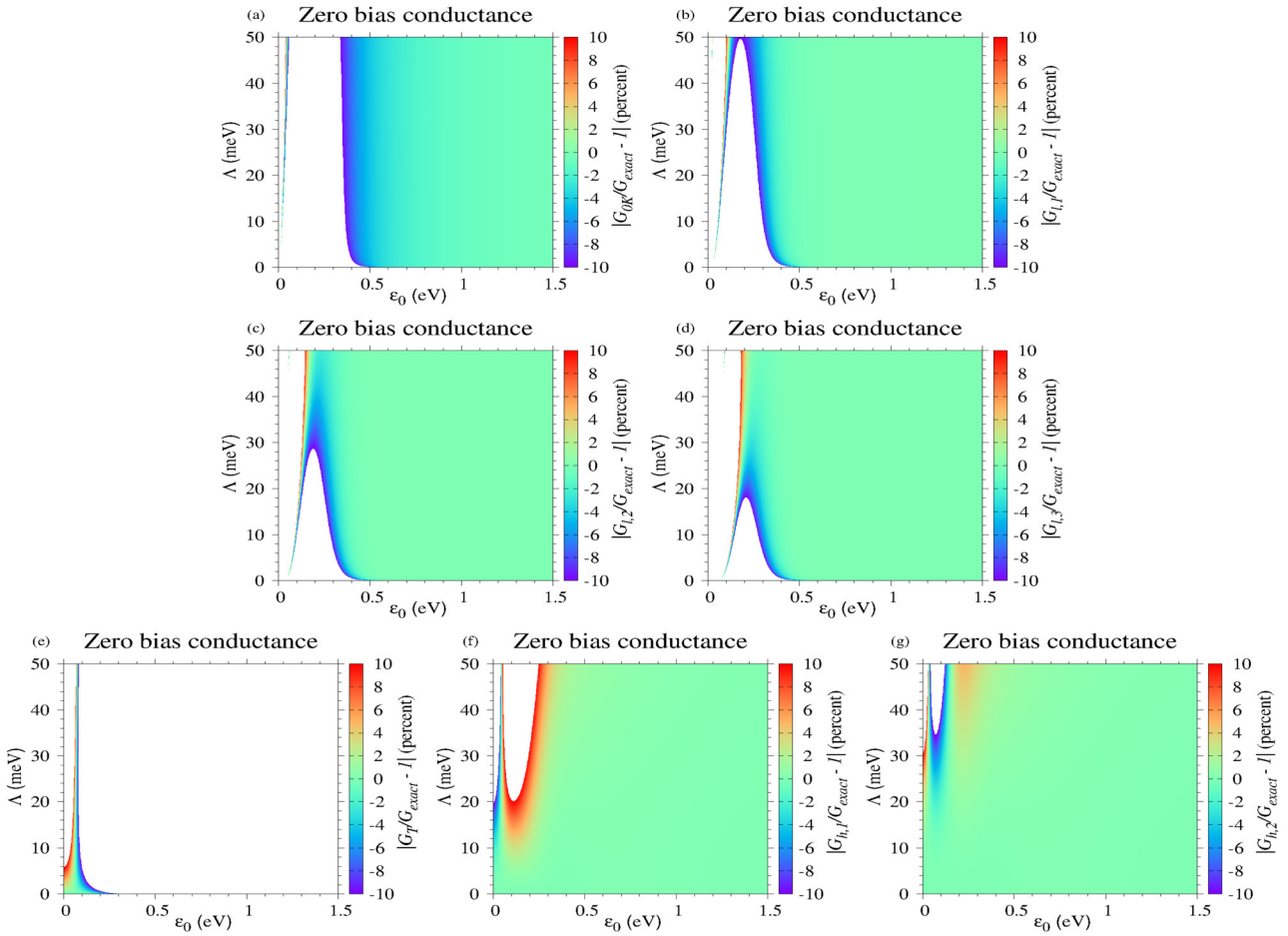

Fig. 6 Percentage deviations of the zero bias conductance computed by the various methods indicated in each of the panels a to g with respect to the value computed exactly at T = 373.15 K.

($j_{0K} \approx j_{exact}$, *cf.* Fig. 10c), and that the transport in off-resonant situations can be reliably described by $j_{0K,off}$ ($\approx j_{exact}$, see green curve in Fig. 10b).

6.1 Working equations for large area EGaIn junctions

Let us first recast eqn (5), (6) and (13) in a form more specific for junctions whose molecules are chemisorbed on a gold substrate (label c,Au) and physisorbed on EGaIn top electrode (label p,EGaIn) or CP-AFM gold tip (label p,Au)

$$\Gamma^2 \to \Gamma_{c,Au|p,EGaIn}{}^2 = \Gamma_{c,Au}\Gamma_{p,EGaIn} = \frac{\bar{\Gamma}^2}{f\Sigma} \tag{14a}$$

$$\Gamma_{p,EGaIn} = \Gamma_{c,Au} \underbrace{\frac{\Gamma_{p,Au}}{\Gamma_{c,Au}}}_{r_1=1/37} \underbrace{\frac{\Gamma_{p,EGaIn}}{\Gamma_{p,Au}}}_{r_2=1/7} \tag{14b}$$

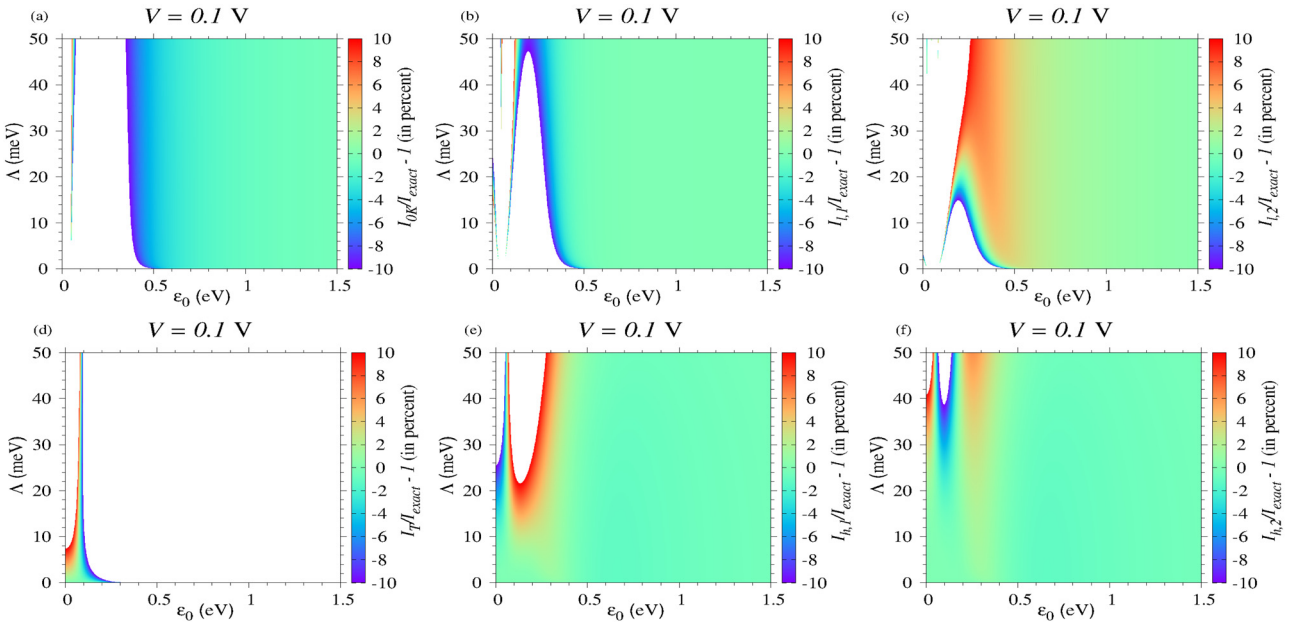

Fig. 7 Percentage deviations of the current computed at V = 0.1 V and T = 373.15 K by the various methods indicated in each of the panels a to f with respect to the value computed exactly.

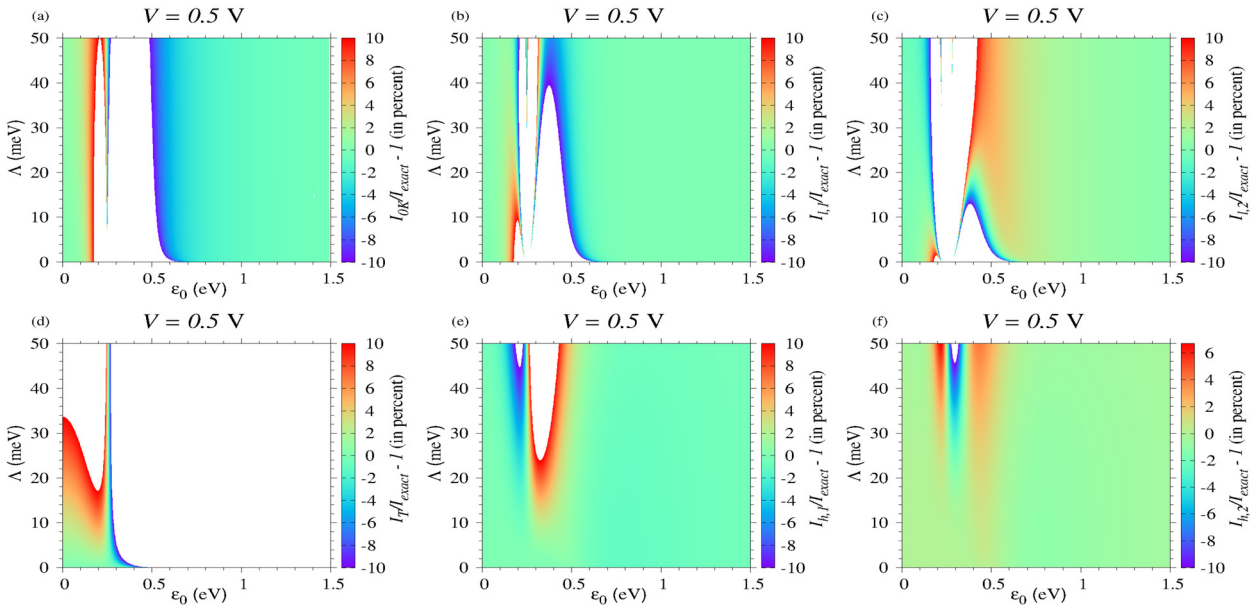

Fig. 8 Percentage deviations of the current computed at V = 0.5 V and T = 373.15 K by the various methods indicated in each of the panels a to f with respect to the value computed exactly.

(from ref. 53)

$$\Gamma_{\mathrm{c,Au|p,Au}} \equiv \sqrt{\Gamma_{\mathrm{c,Au}}\Gamma_{\mathrm{p,Au}}} = 118\ \mu\mathrm{eV} \tag{14c}$$

(*via* ref. 75)

$$\Lambda = \frac{1}{2}\left(\Gamma_{\mathrm{c,Au}} + \Gamma_{\mathrm{p,EGaIn}} + \Gamma_{\mathrm{env}}\right) \tag{14d}$$

Above, $\Gamma_{\mathrm{c,Au|p,EGaIn}}$ and $\Gamma_{\mathrm{c,Au|p,Au}}$ are effective couplings (*cf.* Section 2) of junctions chemisorbed on gold substrate and physisorbed on EGaIn and gold top electrodes, respectively. Γ's with subscripts without vertical bar stand for individual HOMO-electrode couplings (recall that alkanethiols CnT exhibit p-pype HOMO-mediated conduction[75]); *e.g.*, $\Gamma_{\mathrm{p,X}}$ means p(hysical) coupling to electrode X(= Au,EGaIn). Let us now explain how we arrived at the numerical values entering eqn (14b) and (14c).

The coupling ratios $r_{1,2}$ of eqn (14b) were estimated recently.[53] The value of $r_1 \approx 1/37$ was deduced by comparing

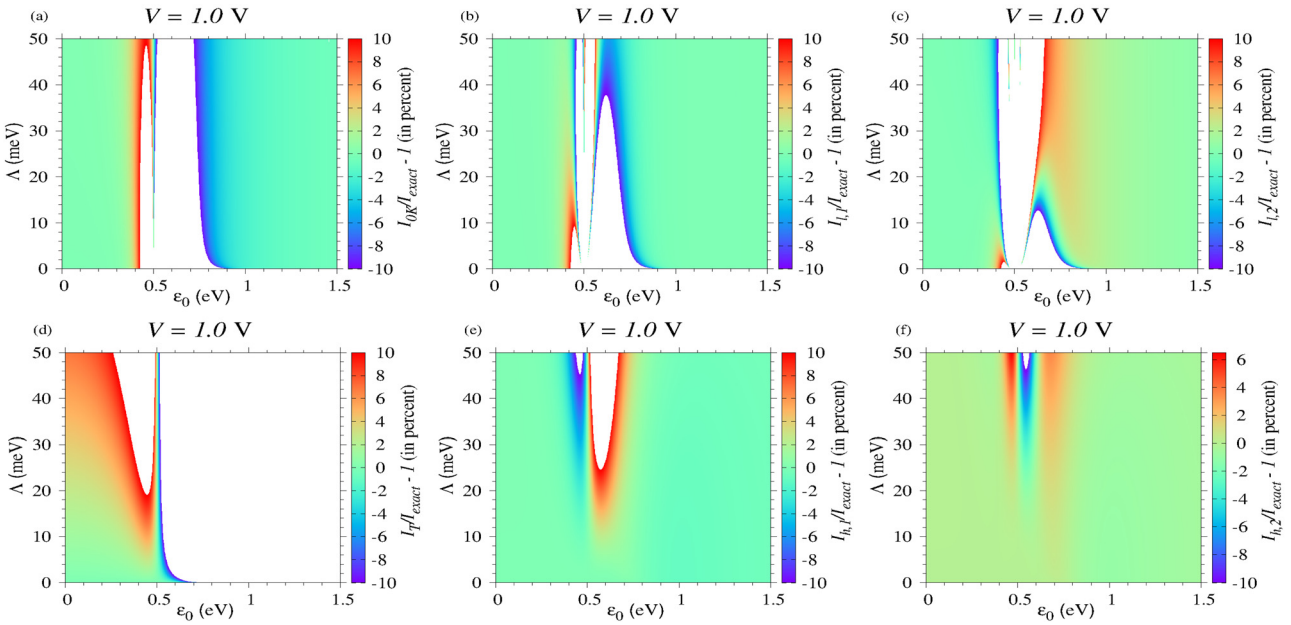

Fig. 9 Percentage deviations of the current computed at V = 1.0 V and T = 373.15 K by the various methods indicated in each of the panels a to f with respect to the value computed exactly.

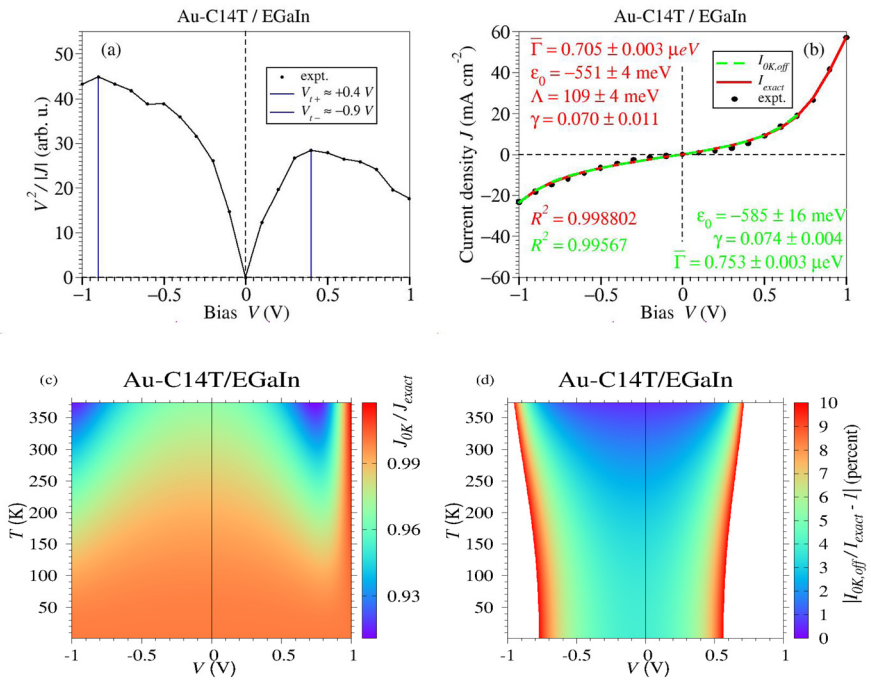

Fig. 10 (a) Plots of $V^2/|I|$ *versus* V enabling the determination of the values of the transition voltages $V_{t\pm}$ needed to properly define the bias range where eqn (12b) applies. (b) Correctly utilized, eqn (12b) is able to reproduce (green curve) the experimental data (black points) for the large area Au-C14T/EGaIn junction of ref. 70 with an accuracy comparable to that of the exact eqn (12a) (red curve). Diagrams revealing (c) that thermal effects are negligible in the Au-C14T/EGaIn junction envisaged and (d) that, when applied for the bias range for it was devised,[43] eqn (12b) is able to describe quantitatively I–V data in large area junctions. See the main text for details.

the couplings of alkane thiols and alkane dithiols. The value of $r_2 \approx 1/7$ relies on the dependence of the coupling on the electrode work function.

To get $\Gamma_{c,Au|p,Au}$ = 118 μeV in eqn (14c), we extrapolated the values of the effective coupling $\Gamma^{(n)}_{c,Au|p,Au} \rightarrow \Gamma_n \propto \exp(-\beta n/2)$ for CP-AFM alkanethiols CnT (H–S–$(CH_2)_{n-1}$–CH_3) junctions

Table 1 Model parameter values obtained by fitting the experimental J–V data[70] to the formulas for the current indicated in the first column

Method	ε_0 (eV)	Λ (meV)	$\bar{\Gamma}$ (μeV nm^{-1})	γ	f	Γ_{env}	$\Gamma_{\mathrm{env}}/(2\Lambda)$ (%)	R^2
J_{exact}	-0.551 ± 0.004	109 ± 0.004	0.705 ± 0.003	0.07 ± 0.01	4.3×10^{-4}	217.3	99.7	0.998802
$J_{0\mathrm{K}}$	-0.535 ± 0.004	115 ± 0.004	0.695 ± 0.002	0.07 ± 0.01	4.2×10^{-4}	229.3	99.7	0.99884
$J_{0\mathrm{K,off}}$	-0.585 ± 0.004	—	0.753 ± 0.003	0.074 ± 0.004	4.9×10^{-4}	—	—	0.99567

(Au–CnT/Au). That is, we used the values of Γ_n (for n = 7, 8, 9, 10, 12) from Table 1 of ref. 75. The exponential scaling of Γ_n *versus* n follows from the exponential falloff $G_n \propto \exp(-\beta n)$ of the low bias conductance $G_n \propto {\Gamma_n}^2/(\varepsilon_0^n)^2$, given the fact that the HOMO offset $\varepsilon_0^{(n)}$ of the CnT series is independent of size (n).[75]

6.2 Estimating the fraction of current carrying molecules and the extrinsic HOMO relaxation

We will now explain how to use the values of $\bar{\Gamma}$ and Λ obtained from I–V data fitting and the above working equations to estimate the fraction of the current carrying molecules f and the extrinsic contribution to the (HO)MO broadening Γ_{env}.

6.2.1 Fraction of current carrying molecules *f*. From the definition of r_1 of eqn (14b), we use eqn (14c) to compute $\Gamma_{\mathrm{c,Au}} = \Gamma_{\mathrm{c,Au|p,Au}}/\sqrt{r_1} = 718$ μeV. Using again the definition of r_1, we deduce $\Gamma_{\mathrm{p,Au}} = \Gamma_{\mathrm{c,Au|p,Au}}\sqrt{r_1} = 3.2$ μeV. From the definition of r_2 of eqn (14b) we get $\Gamma_{\mathrm{p,EGaIn}} = r_2\Gamma_{\mathrm{p,Au}} = 0.456$ μeV. From eqn (14a) we can now compute $\Gamma_{\mathrm{c,Au|p,EGaIn}} = \sqrt{\Gamma_{\mathrm{c,Au}}\Gamma_{\mathrm{p,EGaIn}}} = 18.1$ μeV. With the value Σ = 3.5 mol nm^{-2} measured for the molecular coverage of alkanethiol SAMs,[76] and the fitting parameter value $\bar{\Gamma}$ = 0.705 μeV (Table 1), we can finally estimate *via* eqn (14a) the fraction of the current carrying molecules

$$f_{\mathrm{Au\text{-}C14T/EGaIn}} \approx 4.3 \times 10^{-4}$$

This value is on the same order of magnitudes of other values of f reported for large area EGaIn-based junctions using methos completely different from the present one.[20,53,77] Definitely, out of the total/geometric/nominal area at the EGaIn contact $\mathscr{A}_{\mathrm{n}}$, the area of the physical/electric/effective contact $\mathscr{A}_{\mathrm{eff}} = f\mathscr{A}_{\mathrm{n}}$ is but a tiny fraction ($f \ll 1$).

6.2.2 Extrinsic contribution Γ_{env} to the (HO)MO width. With the values for Λ (Table 1), $\Gamma_{\mathrm{c,Au}}$, and $\Gamma_{\mathrm{p,EGaIn}}$ in hand, we use eqn (14d) and obtain $\Gamma_{\mathrm{env}} \approx 217.3$ meV. This is a very important result. It demonstrates that the extrinsic contribution represents $(\Gamma_{\mathrm{env}}/2)/\Lambda \approx 99.7\%$ of the total HOMO width. Compared to the contribution of the surrounding, the contribution of the electrodes the the HOMO broadening is completely negligible. To obtain the aforementioned values of f and Γ_{env} we used the values of $\bar{\Gamma}$ and λ obtained by fitting the experimental I–V data[70] to the exact eqn (12a). The values collected in Table 1 reveal that these values do not significantly differ from the estimates for f and Γ_{env} based on eqn (12b).

To end, it is worth emphasizing that the off-resonant single level model (eqn (12c)[43]) is also useful for large area EGaIn junctions. Eqn (12c) does not only reproduce I–V curves in nonlinear regime (green line in Fig. 10b) but also allows to reasonably estimate the fraction of current carrying molecules. The rather minor difference between the value $f = 4.9 \times 10^{-4}$ based on eqn (12c) and the "exact" value $f = 4.3 \times 10^{-4}$ deduced *via* eqn (12a) is due to the fact, albeit smaller than $|\varepsilon_0|$, Λ is not smaller that $|\varepsilon_0|/10$, which is the condition for eqn (12c) to be very accurate.[57,58]

7 Predicting a bias-tuned Sommerfeld–Arrhenius transition in a real molecular tunnel junction

Let us now switch to a mechanically controlled break junction (MC-BJ) of 4,4′-biscyanotolane (BCT) with gold electrodes.[54] Results for this junction are collected in Fig. 11. Fitting the digitized I–V data measured at room temperature (Fig. 1 of ref. 54) to eqn (7) at T = 298.15 K yielded an excellent fitting curves (R^2 = 0.994, *cf.* Fig. 11a).

Within the bias range sampled in experiment ($|V| < 0.7$ V),[54] thermal effects are non-negligible (thermal excess higher than 10%) only at the ends of the experimental range: $|V| > V_{10\%} = 0.607$ V ($eV_{10\%} \approx 2(|\varepsilon_0| - 3\pi k_{\mathrm{B}}T) \approx 2(|\varepsilon_0| - 10k_{\mathrm{B}}T)$); see Fig. 11b. Except for biases very close to the highest experimental bias (V = 0.7 V), even the zero temperature expressions ($I_{0\mathrm{K}}$ and $I_{0\mathrm{K,off}}$) are accurate; see Fig. 11e and f. For such situations, the low temperature expansion ($I_{\mathrm{l},1}$, $I_{\mathrm{l},2}$, and $I_{\mathrm{l},3}$) provides an improved description over the zero temperature description ($I_{0\mathrm{K}}$ and $I_{0\mathrm{K,off}}$, see Fig. 11b). More significant is however the high accuracy of the high-temperature approximations: at the small value $\Lambda = 1.71 \pm 0.01$ meV $\ll k_{\mathrm{B}}T = 25.7$ meV obtained by data fitting, even the lowest order expansion ($I_{\mathrm{h},1}$) excellently reproduces the exact current I_{exact}; higher order corrections embodied in $I_{\mathrm{h},2}$ are superfluous.

Beyond the bias range explored in ref. 54, the thermal current enhancement $I_{\mathrm{exact}}/I_{0\mathrm{K}}$ becomes more and more pronounced as the resonance value is approached from below ($eV \lesssim 2|\varepsilon_0|$) and the temperature is increased. Results up to the highest temperature of potential practical interest (T = 373.15 K) are presented in Fig. 11c–e. They show that for biases sufficiently close to resonance, values up to $I_{\mathrm{exact}}/I_{0\mathrm{K}} \approx 20$ can be reached. In such situations, a gradual Arrhenius–Sommerfeld transition[52] can become observable (Fig. 11d).

In Table 2, we collect the model parameters ε_0 (<0, HOMO conduction), Λ (= Γ, single-molecule junction fabricated with a symmetric molecular species) estimated from data fitting to the various formulas for the current. As visible there, applying the zero temperature formulas ($I_{0\mathrm{K}}$ and $I_{0\mathrm{K,off}}$) to situations not enough far away from resonance and $\Lambda \ll k_{\mathrm{B}}T$ yielded an error of 22% in the value estimated for the HOMO offset and 15% for Γ.

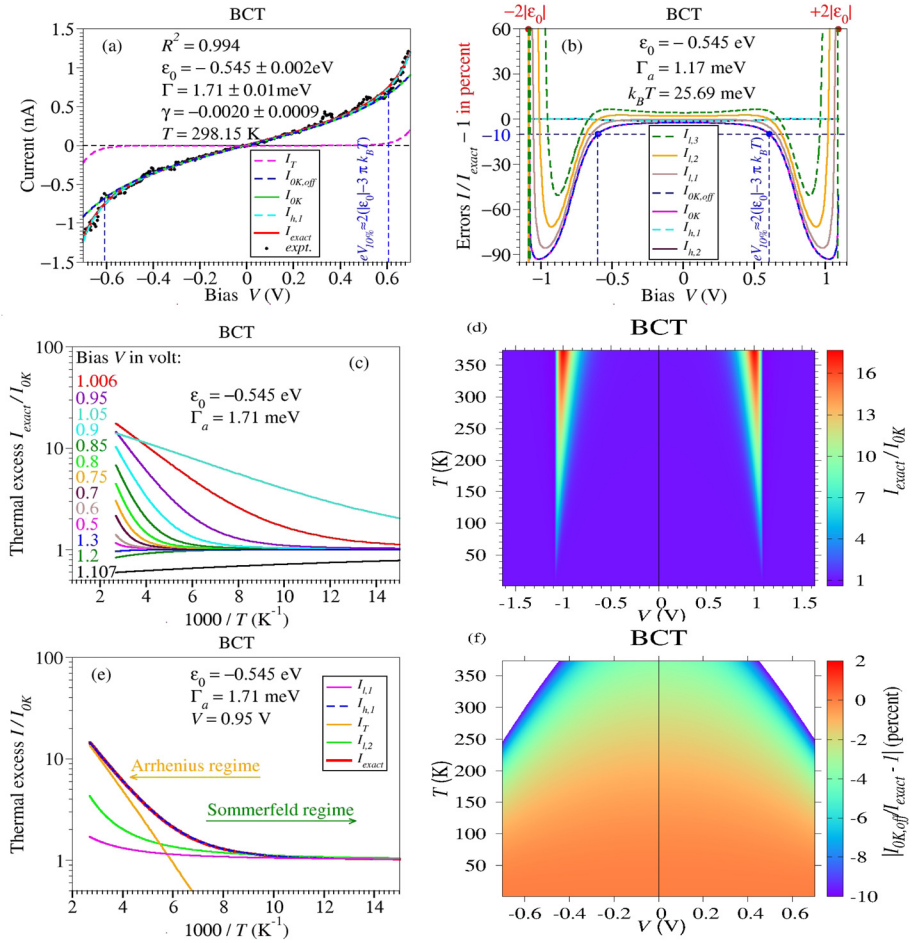

Fig. 11 (a) The experimental I–V curve for a 4,4′-biscyanotolane (BCT) mechanically controlled break junction (MC-BJ) obtained by digitizing Fig. 1 of ref. 54 is excellently fitted by the theoretical current I_{exact} given by eqn (7) at T = 298.15 K. Curves computed using various approximate formulas for current with the optimized model parameters (see legend) are also presented. (b) Percentage deviations from the exact current of the current computed using the methods indicated in the legend shown in a bias range broader than the the bias range explored in experiment (depicted by vertical dashed lines). The thermal excess current I_{exact}/I_{0K} depicted (c) as a function of temperature (T) at several bias values (V) and (d) in the (V, T)-plane. Notice the large values of I_{exact}/I_{0K} in situations slightly below resonance. (e) At biases slightly below resonance (V = 0.95 V, $eV \lesssim 2|\varepsilon_0|$) I_{exact} switches from a weakly T-dependent (Sommerfeld) regime to a strongly T-dependent (Arrhenius-like) regime wherein it can be approximate by the expressions deduced for the low and high T limits, respectively. (f) Regions in the (V, T)-plane where eqn (8b) is accurate within the experimental accuracy.

8 Remarks on the applicability of presently deduced formulas

Going through the plethora of equations presented above, an experimentalist less interested in how they were mathematically deduced may ask what is the appropriate formula needed and how to proceed in transport data processing for a specific junction, fabricated with a specific molecule, specific electrodes, and a specific platform. This section and the next two sections aim at addressing such legitimate questions. Basically, within the model parameter ranges indicated, the formulas of Sections 2, 3 and 5 are general:

8.1 With regard to electrodes

They apply to all electrodes having flat conduction bands around the Fermi energy E_F *i.e.*, having a density of states practically independent of energy $\rho(\varepsilon) \approx \rho(E_F)$. This translates into energy independent MO-electrode couplings ($\Gamma_{s,t}(\varepsilon) \approx \Gamma_{s,t}(E_F) \propto \rho(E_F)\tau_{s,t}^2$, see below). While this is not the case of semiconductors or graphene, it is definitely the case of all typical metals (like Ag, Au, Pt).[78]

8.2 With regard to molecules

The formulas apply to all molecules wherein the charge transport is dominated by a single level (MO), which is in most cases either the HOMO or the LUMO. The applicability of the single level description is often justified intuitively by the sufficiently large energy separation from the adjacent MOs. In fact, MOs' energetic separation may be a sufficient condition but is not a necessary condition. If, in some cases, a few highest occupied (*e.g.*, HOMO and HOMO−1) or a few lowest unoccupied (*e.g.*, LUMO and LUMO+1) have energies close to each other, they typically have different symmetries and/or different spatial (de)localization. The result is that, out of each group (of

Table 2 Model parameter values obtained by fitting the experimental BCT data[54] to the various formulas for the current, as indicated in the first column

Method	ε_0 (eV)	$\Gamma = \Lambda$	γ	R^2
I_{exact}	−0.545 ± 0.002	1.71 ± 0.01	−0.0021 ± 0.0009	0.993551
$I_{h,1}$	−0.547 ± 0.002	1.73 ± 0.01	−0.0021 ± 0.0009	0.993513
$I_{h,2}$	−0.547 ± 0.002	1.72 ± 0.01	−0.0021 ± 0.0009	0.993513
I_{0K}	−0.472 ± 0.004	1.46 ± 0.02	−0.003 ± 0.001	0.992632
$I_{0K,off}$	−0.472 ± 0.004	1.46 ± 0.02	−0.003 ± 0.001	0.992632
$I_{l,1}$	−0.492 ± 0.004	1.50 ± 0.02	−0.003 ± 0.001	0.992729
$I_{l,2}$	−0.511 ± 0.003	1.55 ± 0.02	−0.003 ± 0.001	0.992809
$I_{l,3}$	−0.526 ± 0.003	1.58 ± 0.02	−0.003 ± 0.001	0.992860

occupied or unoccupied MOs), only one MO has significantly overlap with the electronic states in metals. Due to different symmetry (and/or (de)localization) it can happen, *e.g.*, that the (more distant from E_F) HOMO−1 rather than the (closer to E_F) HOMO has a larger hybridization with the single-electron states in the substrate (or tip/top) electrode. A larger hybridization means a transfer integral τ_s quantifying the charge transfer between HOMO−1 and substrate larger than that of the charge transfer between HOMO and substrate. This translates into MO–substrate (or tip) coupling $\Gamma_{s,t} \propto \rho(E_F)\tau_{s,t}{}^2$ dominated by the HOMO-1 and not by the HOMO.

8.3 With regard to the fabrication platform

With appropriate model parameter values (to be adequately estimated from data fitting), these formulas can be applied for molecular junctions fabricated using any platform, let it be MC-BJ, STM-BJ, CP-AFM or (as we have just seen in Section 6) EGaIn. It may be helpful to recall[53] here that, like the model proposed in ref. 43, the present single level model does not assume negligible intermolecular interactions. An electron that tunnels across a molecule can interact with the adjacent molecules. Provided that electron exchange (transfer) between adjacent molecules is absent, the single level model "allows" intermolecular interactions to give rise to an extra MO shift (thence possible different values of ε_0 for single-molecule, CP-AFM, and EGaIn junctions, a fact which will reflect itself in the best fitting estimates) and an extra level broadening expressed by Γ_{env}.[53] This is the rationale of "simply" multiplying the present expressions for current through a single molecule by the number of molecules per junction, as done earlier in case of CP-AFM junctions[75,79,80] or in arriving at eqn (12) above.

9 Protocol for studying a specific junction

In view of the results presented above, assuming that room temperature *I–V* measurements for a specific molecular junction are available (which is the common case), we recommend the following steps for data processing: (i) start by plotting the measured data in coordinates $(V^2/|I|,V)$ and determine the transition voltages $V_{t\pm}$ from the peak location (*cf.* Fig. 10a). Use our eqn (6) and (7) of ref. 43 (reproduced below for the reader's convenience) to estimate the magnitude of the MO offset $|\varepsilon_0|$ and γ

$$|\varepsilon_0| = 2\frac{V_{t+}|V_{t-}|}{\sqrt{V_{t+}{}^2 + 10V_{t+}|V_{t-}|/3 + V_{t-}{}^2}}$$

$$\gamma = \frac{\operatorname{sign}\varepsilon_0}{2}\frac{V_{t+} + |V_{t-}|}{\sqrt{V_{t+}{}^2 + 10V_{t+}|V_{t-}|/3 + V_{t-}{}^2}}$$

The MO offset ε_0 is negative for p-type (normally, HOMO) conduction and positive for n-type (normally, LUMO) conduction. Recall that, whatever the formulas for the current utilized, the sign of ε_0 cannot be merely determined from *I–V* curves measured for a given junction (= given molecule, given electrodes). Thermopower experiments to determine the sign of the Seebeck coefficient S or investigating junctions fabricated with a given molecule and electrodes having different work functions Φ.[75,79,80] may settle this issue; positive (negative) S means negative (positive) ε_0,[81] higher (lower) current for larger Φ means negative[75,79,80] (positive[32]) ε_0.

Determine next the value of $\Gamma = |\varepsilon_0|\sqrt{G/G_0}$ using the low bias conductance G obtained from the slope of the measured *I–V* curve at low bias. With the values of ε_0, Γ and γ thus obtained compare the measured curve with the simulated curve computed using our eqn (8b) in the bias range $-1.2|V_{t-}| \lesssim V \lesssim 1.2V_{t+}$. Alternatively, always in the bias range indicated (for which eqn (8b) applies), one can fit the measured data to $I_{0K\text{-}off}$ of eqn (8b) wherein ε_0, Γ and γ are adjustable parameters. (ii) If attempt (i) fails to produce a good theoretical curve, fit data to I_{0K} of eqn (8a) in the entire bias accessed experimentally with ε_0, Γ, γ, and Λ as adjustable parameters. If the corresponding point $(\varepsilon_0^{0K}, \Lambda^{0K})$ falls in the colored regions of Fig. 6a, 7a, 8a or 9a, this is evidence that the best fit values ε_0^{0K}, Γ^{0K}, γ^{0K} and Λ^{0K} are reliable and that, at the corresponding bias, eqn (8a) is reliable. In other words, at the envisaged bias, thermal corrections to the current are negligible. Notice that (like eqn (8b) and (8a)) can hold up to a certain bias (*e.g.*, V = 0.5 V) but can become inadequate at higher biases (*e.g.*, V = 1 V) (see the example of Section 7). (iii) The failure of attempt (ii) indicates that (possibly only beyond certain biases) the temperature dependence of the current is significant. Generally speaking, whenever possible (*e.g.*, using MATHEMATICA) fitting data to the exact eqn (7) is then most advisable. Otherwise the various analytical formulas for the current $I_{l,1}$, $I_{l,2}$, $I_{l,2}$ of eqn (9) or $I_{h,1}$, $I_{h,2}$ of eqn (10) can be easier applied. Because they merely contain elementary functions the approximate formulas for $I_{l,1}$, $I_{l,2}$, $I_{l,2}$, $I_{h,1}$, and $I_{h,2}$ are implementable in any fitting software package. Loosely speaking, the deeper the point $(\varepsilon_0^{0K}, \Lambda^{0K})$ into the white (non-colored) regions mentioned under (ii) above, the stronger is the impact of T on the current at the corresponding bias. (iii_a) For cases wherein the point $(\varepsilon_0^{0K}, \Lambda^{0K})$ lies near the edge between colored and non-colored regions of Fig. 6a, 7a, 8a, or 9a, thermal effects are rather weak, and using the formula of $I_{l,1}$ of eqn (10g) for data fitting is advisable. If the best fitting point $(\varepsilon_0^{l,1}, \Lambda^{l,1})$ obtained fitting the experimental *I–V* curve to eqn (10h) is found in the colored regions of Fig. 6b, 7b, 8b, or 9b $I_{l,1}$ provides an accurate description and the fitting parameters $\varepsilon_0^{l,1}$, $\Gamma^{l,1}$, $\gamma^{l,1}$, and $\Lambda^{l,1}$ are good estimates of the corresponding quantities. Otherwise,

performing and inspecting the results of data fitting based on $I_{l,2}$ of eqn (9c) (and then $I_{l,3}$ of eqn (9d) if the case) follows in the next step. (iii_b) If the point (ε_0^{0K}, Λ^{0K}) lies deep inside the white (non-colored) regions of Fig. 6a, 7a, 8a, or 9a, thermal effects are strong, and the formula deduced *via* high temperature expansions ($I_{h,1}$ of eqn (10g)) and $I_{h,2}$ of eqn (10h) should be employed for reliably estimate the parameters ε_0, Γ, γ, and Λ for the junction under investigation. In cases where (iii_b) applies, performing *I–V* measurements at variable temperature is highly desirable, and the issues related to the Sommerfeld–Arrhenius transition addressed in the next section deserve consideration.

10 Tunneling-throughout Sommerfeld–Arrhenius scenario *versus* tunneling-hopping transition: a too challenging a dilemma?

For a Sommerfeld–Arrhenius transition to occur in a specific molecular junction, the parameters ε_0 and Λ at given bias V should fall in regions in the plane (ε_0, Λ) where the current thermal enhancement I_{exact}/I_{0K} is sufficiently large (say, at least $I_{exact}/I_{0K} \gtrsim 10$), like the red curve in (Fig. 11e). The color coding of Fig. 6a, 7a, 8a, or 9a precisely depicts which combination of values (ε_0,Λ,V) is "eligible" for a Sommerfeld–Arrhenius transition (*i.e.*, I_{exact}/I_{0K} is reasonably large). Experimental curves for current *versus* inverse temperature having a shape resembling the red curve in Fig. 11e have been measured in the past for several molecular junctions. Examples include junctions fabricated with: conjugated oligo-tetrathiafulvalenepyromelliticdiimideimine (OPTIn; OPTI2 in Fig. 6a in ref. 5), bis-thienylbenzene (BTB; Fig. 3c and 4 in ref. 11), cytochrome *C* and hemin-doped human serum albuminum (HSA-hemin) (Cyt *C* and HSA-hemin; Fig. 6a and b in ref. 12), and closed and open diarylethene isomers (Fig. 2c and d in ref. 30). Out of the cases cited, only ref. 11 reported attempts (that failed) of quantitatively fitting the measured curve of *I versus* $1/T$ to a theoretical model that could come into question, namely the variable hopping range model[82–84] and the classical Poole–Frenkel model for transport between coulombic traps.[85,86] Based on the previous knowledge in the field, all the aforementioned data were interpreted as evidence of a tunneling-hopping transition. However, this interpretation needs to be reconsidered, and all the more so since the present theory of the Sommerfeld–Arrhenius scenario provides a unique formula that can be applied for the entire temperature and bias ranges accessed experimentally. A dilemma may arise in cases where the measured current *I* follows an Arrhenius pattern at high *T* and eventually switches to *T*-independent values at low *T*: is the dependence $I \propto \exp\left(-\frac{E_a}{k_B T}\right)$ at high *T* due to thermally activated hopping or evidence for the strongly *T*-dependent tunneling current discussed in this paper? To differentiate between these two possibilities, in previous studies we suggested investigations of junctions having electrodes with significantly different work function[32,46] or subject to mechanical stretching.[53] The present results indicate two alternatives easier to implement experimentally in order to differentiate between strongly *T*-dependent tunneling and hopping: (a) To unravel the physics underlying an observed switching from strong *T*-dependent to *T*-independent (or weak *T*-dependent) currents, *I–V* curves measured at low temperatures can be fitted to eqn (8) assuming *T*-independent *I* (or eqn (9) assuming weak *T*-dependent *I*). The value $|\varepsilon_0|$ of the MO offset thus obtained can be compared:

(a_1) with the value of the "activation energy" E_a obtained by fitting the high temperature data to the Arrhenius law $I \propto \exp\left(-\frac{E_a}{k_B T}\right)$. An E_a significantly different from $|\varepsilon_0|$ is evidence for hopping-tunneling transition, $|\varepsilon_0| \approx E_a$ pleads for a tunneling-throughout Sommerfeld–Arrhenius scenario.

(a_2) with the value of the MO offset $|\varepsilon_{1/2}|$ obtained *via* ultraviolet photoelectron spectroscopy (UPS). Obviously, this makes sense in case of p-type conduction, where evidence exists that the "second" (tip) electrode negligibly affect the level alignment ($\varepsilon_{1/2} \approx \varepsilon_0$), which is basically the same for full and "half" (*i.e.* only SAM adsorbed on substrate without tip/top electrode) junctions.[75,79,80] For n-type conduction determining the (LU)MO offset $\varepsilon_{1/2}$ *via* inverse photoelectron spectroscopy (IPS) could come into question.

(b) To start with a specific example, let us consider again the BCT junction of Section 7 and compare the ratio of the currents at room temperature and at liquid nitrogen $I_{RT}/I_{LN}|_V \equiv I(V,298.15\ K)/I(V,77\ K)$ computed using the exact eqn (7) for several biases *V*: $I_{RT}/I_{LN}|_{V=1V} = 11.38$; $I_{RT}/I_{LN}|_{V=0.9V} = 5.55$; $I_{RT}/I_{LN}|_{V=0.8V} = 2.20$; $I_{RT}/I_{LN}|_{V=0.7V} = 1.31$; $I_{RT}/I_{LN}|_{V=0.6V} = 1.10$; $I_{RT}/I_{LN}|_{V=0.5V} = 1.05$; $I_{RT}/I_{LN}|_{V=0.4V} = 1.03$; $I_{RT}/I_{LN}|_{V=0.4V} = 1.02$. These values show an almost exponential decrease in the thermal enhancement I_{RT}/I_{LN} in the narrow bias range $0.7\ V \lesssim V \lesssim 1\ V$ slightly below resonance ($eV_{resonance} = 2|\varepsilon_0| \simeq 1.1$ V). By contrast, sufficiently away from resonance ($V \lesssim 0.6$ V) the thermal enhancement is practically negligible ($I_{RT}/I_{LN}|_{V\lesssim 0.6V} \approx 1$). This example illustrates that the Sommerfeld–Arrhenius transition is bias sensitive. In a given junction, a Sommerfeld–Arrhenius transition is observable at some biases while at other biases it cannot be observed. Such a bias sensitivity could not be expected if hopping dominated at higher temperature. The thermal activation energy is mainly determined by molecular properties (*e.g.*, reorganization energy) which are little sensitive to external bias.

To sum up, by and large, data measured over a broad range of biases exhibiting a similar pattern (gradual transition between two distinct regimes) plead for a tunneling-hopping transition. Otherwise (*i.e.*, if switching between a weak temperature dependence at low *T* to a strong *T* dependence at high *T* mainly occurs in a narrow range of *V*, see Fig. 11c) an overall tunneling picture applies; the temperature dependence is merely the result of thermally broadened Fermi distributions.

11 Conclusion

We hope that the various analytical formulas for the tunneling current reported here will assist experimentalists to adequately

process transport data measured at nonvanishing (room) temperature and to more properly assign the transport mechanism at work in a specific molecular junction. Letting alone the aspect of elegance, the present analytical formulas have an important practical advantage over the often utilized brute force method of numerically integrating eqn (4) using a uniform energy grid. To resolve both the thermal smearing of the Fermi distributions and the variation of transmission with energy, a sufficiently fine uniform energy grid requires an energy step size $\delta\varepsilon \approx \min(k_BT,\Lambda)/10$. In an energy range $\Delta\varepsilon \sim 10$ eV this easily translates into a grid with $N \sim 10^4$–10^6 points, which may make data fitting time consuming in some cases.

To be sure, adaptive numerical quadrature can alternatively be employed, and it is to be preferred to the brute force approach. Still, in spot checks to reproduce the present exact results obtained *via* eqn (7), we had to conclude that applying adaptive numerical quadrature to eqn (4) with default settings (precision goal, working precision, *etc.*) using current distributions of MATHEMATICA (13.2.1) and MATLAB (R2021a) also poses nontrivial numerical problems for small Λ and k_BT (k_BT, $\Lambda \lesssim 1$ meV).

Based on the results reported in this paper, for experimentalists unable to use eqn (7) to data fitting—*e.g.*, because neither MATLAB nor ORIGIN can handle digamma function of complex argument—we recommend utilization of eqn (10g) and (9c), which provide a accurate description that complimentary covers most situations of practical interest. Albeit somewhat lengthy, they merely comprise elementary functions and can be used with any routine fitting software.

A cursory glance at an experimental curve looking like that depicted in Fig. 11d can easily be taken as ''evidence'' of a tunneling-hopping crossover or—in view of the T-dependent slope (''activation energy'')—of a variable variable-range hopping. In reality, we have seen that, it is the tunneling that is at work there both at low and high T. Emphasizing this point, the results reported above aim at aiding the molecular electronics community in not rushing conclude a transition from tunneling to hopping merely based on measured transport properties that switch from nearly temperature independent (Sommerfeld regime) to strongly temperature dependent (Arrhenius-like regime) upon rising the temperature.

The fact that the presently discussed Sommerfeld–Arrhenius can be tuned by bias can be an important theoretical finding in correctly assessing the physics underlying a curve like that of Fig. 11d.

Not to forget, we have also shown that the single level model considered in this paper is useful not only for single-molecule[54,87,88] and CP-AFM[69,75,79,89] junctions for which it was previously validated. It can also decipher charge transport in large area ($\mathscr{A}_n \approx 500$ μm^2) junctions with EGaIn top electrode. For example, we have shown that, when adequately applied, even our off-resonant single level model[43] can provide a reasonable estimate of the fraction of the current carrying molecules ($f = N_{eff}/N_n = \mathscr{A}_{eff}/\mathscr{A}_n \approx 4 \times 10^{-4}$) in a large area EGaIn junction fabricated with 1-tetradecanethiol.

Conflicts of interest

There are no conflicts to declare.

Acknowledgements

I am pleased to dedicate this paper to Professor Jochen Schirmer on the occasion of his 80th birthday and greatfully acknowledge fruitful interaction extending over many years. Financial support from the German Research Foundation (DFG Grant No. BA 1799/3-2) in the initial stage of this work and computational support by the state of Baden-Württemberg through bwHPC and the German Research Foundation through Grant No. INST 40/575-1 FUGG (bwUniCluster 2, bwForCluster/HELIX, and JUSTUS 2 cluster) are gratefully acknowledged.

References

1 M. Poot, E. Osorio, K. O'Neill, J. M. Thijssen, D. Vanmaekelbergh, C. A. van Walree, L. W. Jenneskens and H. S. J. van der Zant, *Nano Lett.*, 2006, **6**, 1031–1035.
2 X. Li, J. Hihath, F. Chen, T. Masuda, L. Zang and N. Tao, *J. Am. Chem. Soc.*, 2007, **129**, 11535–11542.
3 S. H. Choi, B. Kim and C. D. Frisbie, *Science*, 2008, **320**, 1482–1486.
4 H. Song, Y. Kim, Y. H. Jang, H. Jeong, M. A. Reed and T. Lee, *Nature*, 2009, **462**, 1039–1043.
5 S. H. Choi and C. D. Frisbie, *J. Am. Chem. Soc.*, 2010, **132**, 16191–16201.
6 T. Hines, I. Diez-Perez, J. Hihath, H. Liu, Z.-S. Wang, J. Zhao, G. Zhou, K. Müllen and N. Tao, *J. Am. Chem. Soc.*, 2010, **132**, 11658–11664.
7 I. Diez-Perez, J. Hihath, T. Hines, Z.-S. Wang, G. Zhou, K. Müllen and N. Tao, *Nat. Nanotechnol.*, 2011, **6**, 226–231.
8 G. Sedghi, V. M. Garcia-Suarez, L. J. Esdaile, H. L. Anderson, C. J. Lambert, S. Martin, D. Bethell, S. J. Higgins, M. Elliott, N. Bennett, J. E. Macdonald and R. J. Nichols, *Nat. Nanotechnol.*, 2011, **6**, 517–523.
9 R. Heimbuch, H. Wu, A. Kumar, B. Poelsema, P. Schön, G. J. Vancso and H. J. W. Zandvliet, *Phys. Rev. B: Condens. Matter Mater. Phys.*, 2012, **86**, 075456.
10 R. L. McCreery, H. Yan and A. J. Bergren, *Phys. Chem. Chem. Phys.*, 2013, **15**, 1065–1081.
11 H. Yan, A. J. Bergren, R. McCreery, M. L. D. Rocca, P. Martin, P. Lafarge and J. C. Lacroix, *Proc. Natl. Acad. Sci. U. S. A.*, 2013, **110**, 5326–5330.
12 N. Amdursky, D. Ferber, I. Pecht, M. Sheves and D. Cahen, *Phys. Chem. Chem. Phys.*, 2013, **15**, 17142–17149.
13 K. Asadi, A. J. Kronemeijer, T. Cramer, L. Jan Anton Koster, P. W. M. Blom and D. M. de Leeuw, *Nat. Commun.*, 2013, **4**, 1710.
14 S. Saha, J. R. Owens, V. Meunier and K. M. Lewis, *Appl. Phys. Lett.*, 2013, **103**, 173101.
15 Q. Ferreira, A. M. Bragança, L. Alcácer and J. Morgado, *J. Phys. Chem. C*, 2014, **118**, 7229–7234.

16 O. E. Castañeda Ocampo, P. Gordiichuk, S. Catarci, D. A. Gautier, A. Herrmann and R. C. Chiechi, *J. Am. Chem. Soc.*, 2015, **137**, 8419–8427.
17 L. Xiang, J. L. Palma, C. Bruot, V. Mujica, M. A. Ratner and N. Tao, *Nat. Chem.*, 2015, **7**, 221–226.
18 G. Pace, L. Caranzi, S. G. Bucella, G. Dell'Erba, E. Canesi, C. Bertarelli and M. Caironi, *Nanoscale*, 2014, **7**, 2076–2084.
19 M. Gilbert Gatty, A. Kahnt, L. J. Esdaile, M. Hutin, H. L. Anderson and B. Albinsson, *J. Phys. Chem. B*, 2015, **119**, 7598–7611.
20 D. Taherinia, C. E. Smith, S. Ghosh, S. O. Odoh, L. Balhorn, L. Gagliardi, C. J. Cramer and C. D. Frisbie, *ACS Nano*, 2016, **10**, 4372–4383.
21 C. S. S. Sangeeth, A. T. Demissie, L. Yuan, T. Wang, C. D. Frisbie and C. A. Nijhuis, *J. Am. Chem. Soc.*, 2016, **138**, 7305–7314.
22 Y. Li, L. Xiang, J. L. Palma, Y. Asai and N. Tao, *Nat. Commun.*, 2016, **7**, 11294.
23 L. Xiang, T. Hines, J. L. Palma, X. Lu, V. Mujica, M. A. Ratner, G. Zhou and N. Tao, *J. Am. Chem. Soc.*, 2016, **138**, 679–687.
24 R. L. McCreery, *Beilstein J. Nanotechnol.*, 2016, **7**, 32–46.
25 A. R. Garrigues, L. Yuan, L. Wang, E. R. Mucciolo, D. Thompon, E. del Barco and C. A. Nijhuis, *Sci. Rep.*, 2016, **6**, 26517.
26 A. R. Garrigues, L. Yuan, L. Wang, S. Singh, E. del Barco and C. A. Nijhuis, *Dalton Trans.*, 2016, **45**, 17153–17159.
27 K. S. Kumar, R. R. Pasula, S. Lim and C. A. Nijhuis, *Adv. Mater.*, 2016, **28**, 1824–1830.
28 C. Jia, A. Migliore, N. Xin, S. Huang, J. Wang, Q. Yang, S. Wang, H. Chen, D. Wang, B. Feng, Z. Liu, G. Zhang, D.-H. Qu, H. Tian, M. A. Ratner, H. Q. Xu, A. Nitzan and X. Guo, *Science*, 2016, **352**, 1443–1445.
29 D. Xiang, X. Wang, C. Jia, T. Lee and X. Guo, *Chem. Rev.*, 2016, **116**, 4318–4440.
30 N. Xin, C. Jia, J. Wang, S. Wang, M. Li, Y. Gong, G. Zhang, D. Zhu and X. Guo, *J. Phys. Chem. Lett.*, 2017, **8**, 2849–2854.
31 A. Morteza Najarian and R. L. McCreery, *ACS Nano*, 2017, **11**, 3542–3552.
32 C. E. Smith, Z. Xie, I. Bâldea and C. D. Frisbie, *Nanoscale*, 2018, **10**, 964–975.
33 S. Valianti, J.-C. Cuevas and S. S. Skourtis, *J. Phys. Chem. C*, 2019, **123**, 5907–5922.
34 N. Xin, C. Hu, H. Al Sabea, M. Zhang, C. Zhou, L. Meng, C. Jia, Y. Gong, Y. Li, G. Ke, X. He, P. Selvanathan, L. Norel, M. A. Ratner, Z. Liu, S. Xiao, S. Rigaut, H. Guo and X. Guo, *J. Am. Chem. Soc.*, 2021, **143**, 20811–20817.
35 S. Park, J. W. Jo, J. Jang, T. Ohto, H. Tada and H. J. Yoon, *Nano Lett.*, 2022, **22**, 7682–7689.
36 C. Caroli, R. Combescot, P. Nozieres and D. Saint-James, *J. Phys. C: Solid State Phys.*, 1971, **4**, 916.
37 C. Caroli, R. Combescot, D. Lederer, P. Nozieres and D. Saint-James, *J. Phys. C: Solid State Phys.*, 1971, **4**, 2598.
38 R. Combescot, *J. Phys. C: Solid State Phys.*, 1971, **4**, 2611.
39 W. Schmickler, *J. Electroanal. Chem.*, 1986, **204**, 31–43.
40 I. R. Peterson, D. Vuillaume and R. M. Metzger, *J. Phys. Chem. A*, 2001, **105**, 4702–4707.
41 C. A. Stafford, *Phys. Rev. Lett.*, 1996, **77**, 2770–2773.
42 M. Büttiker and D. Sánchez, *Phys. Rev. Lett.*, 2003, **90**, 119701.
43 I. Bâldea, *Phys. Rev. B: Condens. Matter Mater. Phys.*, 2012, **85**, 035442.
44 J. G. Simmons, *J. Appl. Phys.*, 1963, **34**, 1793–1803.
45 I. Bâldea, *Phys. Chem. Chem. Phys.*, 2015, **17**, 20217–20230.
46 I. Bâldea, *Phys. Chem. Chem. Phys.*, 2017, **19**, 11759–11770.
47 I. Bâldea, *Org. Electron.*, 2017, **49**, 19–23.
48 Z. Xie, I. Bâldea and C. D. Frisbie, *Chem. Sci.*, 2018, **9**, 4456–4467.
49 I. Bâldea, *Phys. Rev. B*, 2021, **103**, 195408.
50 Z. Xie, I. Bâldea, Q. Nguyen and C. D. Frisbie, *Nanoscale*, 2021, **13**, 16755–16768.
51 I. Bâldea, *Adv. Theory Simul.*, 2022, **5**, 2200077.
52 I. Bâldea, *Adv. Theory Simul.*, 2022, **5**, 202200158.
53 I. Bâldea, *Int. J. Mol. Sci.*, 2022, **23**, 14985.
54 L. A. Zotti, T. Kirchner, J.-C. Cuevas, F. Pauly, T. Huhn, E. Scheer and A. Erbe, *Small*, 2010, **6**, 1529–1535.
55 H. J. W. Haug and A.-P. Jauho, *Quantum Kinetics in Transport and Optics of Semiconductors*, Springer Series in Solid-State Sciences, Berlin, Heidelberg, New York, second, substantially revised edn, 2008, vol. 123.
56 G. D. Mahan, *Many-Particle Physics*, Plenum Press, New York and London, 2nd edn, 1990.
57 I. Bâldea, *Phys. Chem. Chem. Phys.*, 2023, **25**, 19750–19763.
58 I. Bâldea, Comment on "A single level tunneling model for molecular junctions: evaluating the simulation methods" by Opodi *et al.*, 2023, *Phys. Chem. Chem. Phys.*, DOI: **10.1039/D2CP05110A**, *ChemRxiv*, preprint, DOI: **10.26434/chemrxiv-2023-7fx77**.
59 K. Maki, in *Superconductivity*, ed. R. D. Parks, Dekker, New York, 1969, ch. Gapless Superconductivity, vol. 2, p. 1035.
60 I. Bâldea and M. Bădescu, *Phys. Rev. B: Condens. Matter Mater. Phys.*, 1993, **48**, 8619–8628.
61 I. Bâldea, *Adv. Theory Simul.*, 2022, **5**, 2100480.
62 L. E. Hall, J. R. Reimers, N. S. Hush and K. Silverbrook, *J. Chem. Phys.*, 2000, **112**, 1510–1521.
63 I. Bâldea and H. Köppel, *Phys. Rev. B: Condens. Matter Mater. Phys.*, 2010, **81**, 193401.
64 I. G. Medvedev, *J. Chem. Phys.*, 2017, **147**(19), 194108.
65 *Handbook of Mathematical Functions with Formulas, Graphs, and Mathematical Tables*, ed. M. Abramowitz and I. A. Stegun, National Bureau of Standards Applied Mathematics Series, U.S. Government Printing Office, Washington, D.C., 1964.
66 E. Jahnke and F. Emde, *Tables of Functions with Formulae and Curves*, Dover Publications, 4th edn, 1945.
67 A. Sommerfeld and H. Bethe, in *Handbuch der Physik*, ed. H. Geiger and K. Scheel, Julius-Springer-Verlag, Berlin, 1933, vol. 24(2), p. 446.
68 N. W. Ashcroft and N. D. Mermin, *Solid State Physics*, Saunders College Publishing, New York, 1976, pp. 20–23, 52.
69 Z. Xie, I. Bâldea, A. T. Demissie, C. E. Smith, Y. Wu, G. Haugstad and C. D. Frisbie, *J. Am. Chem. Soc.*, 2017, **139**, 5696–5699.
70 C. M. Bowers, K.-C. Liao, T. Zaba, D. Rappoport, M. Baghbanzadeh, B. Breiten, A. Krzykawska, P. Cyganik and G. M. Whitesides, *ACS Nano*, 2015, **9**, 1471–1477.

71 Y. Selzer, L. Cai, M. A. Cabassi, Y. Yao, J. M. Tour, T. S. Mayer and D. L. Allara, *Nano Lett.*, 2005, **5**, 61–65.
72 F. Milani, C. Grave, V. Ferri, P. Samori and M. A. Rampi, *ChemPhysChem*, 2007, **8**, 515–518.
73 F. C. Simeone, H. J. Yoon, M. M. Thuo, J. R. Barber, B. Smith and G. M. Whitesides, *J. Am. Chem. Soc.*, 2013, **135**, 18131–18144.
74 S. Mukhopadhyay, S. K. Karuppannan, C. Guo, J. A. Fereiro, A. Bergren, V. Mukundan, X. Qiu, O. E. Castaneda Ocampo, X. Chen, R. C. Chiechi, R. McCreery, I. Pecht, M. Sheves, R. R. Pasula, S. Lim, C. A. Nijhuis, A. Vilan and D. Cahen, *iScience*, 2020, **23**, 101099.
75 Z. Xie, I. Bâldea and C. D. Frisbie, *J. Am. Chem. Soc.*, 2019, **141**, 18182–18192.
76 A. T. Demissie, G. Haugstad and C. D. Frisbie, *J. Phys. Chem. Lett.*, 2016, **7**, 3477–3481.
77 H. J. Yoon, C. M. Bowers, M. Baghbanzadeh and G. M. Whitesides, *J. Am. Chem. Soc.*, 2014, **136**, 16–19.
78 D. A. Papaconstantopoulos, *Handbook of the Band Structure of Elemental Solids*, Springer, 2nd edn, 2015.
79 Z. Xie, I. Bâldea, C. Smith, Y. Wu and C. D. Frisbie, *ACS Nano*, 2015, **9**, 8022–8036.
80 Z. Xie, I. Bâldea and C. D. Frisbie, *J. Am. Chem. Soc.*, 2019, **141**, 3670–3681.
81 M. Paulsson and S. Datta, *Phys. Rev. B: Condens. Matter Mater. Phys.*, 2003, **67**, 241403.
82 N. Mott and W. Twose, *Adv. Phys.*, 1961, **10**, 107–163.
83 R. M. Hill, *Philos. Mag.*, 1971, **24**, 1307–1325.
84 R. M. Hill, *Phys. Status Solidi A*, 1976, **34**, 601–613.
85 H. Poole, *London, Edinburgh Dublin Philos. Mag. J. Sci.*, 1916, **32**, 112–129.
86 J. Frenkel, *Phys. Rev.*, 1938, **54**, 647–648.
87 I. Bâldea, *J. Am. Chem. Soc.*, 2012, **134**, 7958–7962.
88 K. Luka-Guth, S. Hambsch, A. Bloch, P. Ehrenreich, B. M. Briechle, F. Kilibarda, T. Sendler, D. Sysoiev, T. Huhn, A. Erbe and E. Scheer, *Beilstein J. Nanotechnol.*, 2016, **7**, 1055–1067.
89 A. Tan, S. Sadat and P. Reddy, *Appl. Phys. Lett.*, 2010, **96**, 013110.

